

CZECH TECHNICAL UNIVERSITY IN PRAGUE

Faculty of Mechanical Engineering

Department of Automotive, Combustion Engine and Railway
Engineering



MASTER THESIS

Effects of operating conditions on the production of brake wear
particles

August 2020

Submitted by: Srinath Penumarti

Supervisor: prof. Michal Vojtisek, Ph.D



MASTER'S THESIS ASSIGNMENT

I. Personal and study details

Student's name: **Penumarti Srinath** Personal ID number: **475374**
Faculty / Institute: **Faculty of Mechanical Engineering**
Department / Institute: **Department of Automotive, Combustion Engine and Railway Engineering**
Study program: **Master of Automotive Engineering**
Branch of study: **Advanced Powertrains**

II. Master's thesis details

Master's thesis title in English:

Effects of operating conditions on the production of brake wear particles

Master's thesis title in Czech:

Vliv provozních podmínek na produkci částic z otěrů brzdového obložení

Guidelines:

Friction brake wear particles are believed to substantially contribute to the adverse health effects of particles emitted by motor vehicles. To evaluate the emissions from current and future materials and technologies, novel particle sampling and measurement systems and also representative testing conditions are evaluated. The goal of the thesis is to analyze online and offline data from a brake wear particle measurement campaign comprising four types of brake pads and various braking conditions. The effects of braking conditions on particle emissions characteristics, such as particle size distribution, or total particle number and mass in different size bins, are to be examined, considering braking intensity, dissipated power and work, friction surface temperatures, and other variables. The results of different measurement instruments should be compared and reconciled. The results are to be discussed and summarized.

Bibliography / sources:

1. Garg, B. D., et al. (2000). Environmental Science & Technology, 34(21), 4463-4469. // 2. Gramstat, S., et al., SAE Int. J. Engines 10(4):1841-1846, 2017. // 3. Hagino, H., et al. (2016). Atmospheric Environment, 131, 269-278. // 4. Kukutschová, J., et al. (2010). Wear, 268(1-2), 86-93. // 5. Martyr, A. J., Plint, M. A. (2012). Engine testing: The design, building, modification and use of powertrain test facilities. // 6. Nosko, O., Olofsson, U., Wear, 374-375, 2017, 92-96.

Name and workplace of master's thesis supervisor:

doc. Michal Vojtíšek, Ph.D., Department of Automotive, Combustion Engine and Railway Engineering, FME

Name and workplace of second master's thesis supervisor or consultant:

Date of master's thesis assignment: **15.06.2020** Deadline for master's thesis submission: **14.08.2020**

Assignment valid until: _____

doc. Michal Vojtíšek, Ph.D.
Supervisor's signature

doc. Ing. Oldřich Vitek, Ph.D.
Head of department's signature

prof. Ing. Michael Valášek, DrSc.
Dean's signature

III. Assignment receipt

The student acknowledges that the master's thesis is an individual work. The student must produce his thesis without the assistance of others, with the exception of provided consultations. Within the master's thesis, the author must state the names of consultants and include a list of references.

Date of assignment receipt

Student's signature

Declaration of authorship

I hereby declare that this diploma thesis has been written by me in person. All the information from other works has been acknowledged in the text with the list of references.

In Prague: 14. 08. 2020

Srinath Penumarti

Abstract

This master thesis deals with the evaluation of particle emissions from four different commercial brake pads for a typical automobile with regards to various braking conditions. A full scale inertia brake dynamometer was used to test the brake pads using portions of standardized test procedures ISO 26867 and SAE J2522 and the newly developed brake WLTC cycle for brake wear particle testing. The particle concentrations were measured online with EEPS and ELPI particle sizers sampling from an outlet duct of the dynamometer enclosure. Particle production per brake event was calculated and the effects of initial and final brake disc temperature and average dissipated power were evaluated. Both the braking intensity and the energy dissipated per brake event had considerable effect on particle production. The particle emissions during WLTC cycle representing real driving were far lower than for more severe, albeit still reasonably realistic, brake events used in standardized procedures.

Keywords: brake-wear, disc brakes, non-exhaust emissions, particle emissions, ISO 26867, SAE J2522, WLTC

Acknowledgement

Firstly, I would like to thank my thesis supervisor prof. Michal Vojtisek, Ph.D., Faculty of Mechanical Engineering, Czech Technical University in Prague, for his outstanding guidance and excellent moral support throughout my thesis work. I would also like to thank all the staff at Technical University of Ostrava who had given the testing facility for carrying out this experiment. I would also like to thank my friends and family members who had supported me for the study at this university. Finally, I would like to thank people working on improving quality of the air and environment continuously.

Contents

1	Introduction	1
1.1	Particulate Matter	1
1.1.1	Particulate Matter Classification.....	2
1.1.2	Mechanism of Particle formation	3
1.2	Effects of PM on human health and Environment.....	5
1.2.1	Ambient Air Quality	6
1.3	Brake.....	8
1.3.1	Brake mechanism.....	8
1.3.2	Brake emissions	9
2	Goal of the Thesis	11
3	Experimental Setup	12
3.1	Brake Dynamometer	12
3.2	Instruments used in the experiment.....	13
3.2.1	Electrical low-pressure impactor (ELPI+)	14
3.2.2	Engine Exhaust Particle Sizer (EEPS)	14
4	Brake Wear Test Procedures	16
4.1	ISO 26867	16
4.2	SAE J2522	17
4.3	Sequence of test procedure.....	18
4.4	WLTC Cycle (Novel Test Cycle)	19
4.5	Comparison of Cycles	20
5	Data Analysis.....	22
5.1	Instrument Signal and Noise	22
5.2	Detection limit.....	23
5.3	Baseline and Peak Calculation.....	25
5.4	Time Synchronization between Instruments	26
5.5	Energy and Power dissipation	27

5.6	Particle Size and Mass Distribution	28
5.6.1	Integrated Particle Size Distribution method (IPSD)	32
5.6.2	ELPI Gravimetric method (offline mass)	33
6	Results.....	34
6.1	Particle emissions of brake pads.....	34
6.2	Particle emissions from F, G, H and K section (EEPS).....	35
6.3	Dissipated Power on Particle emissions.....	41
6.4	Particle emissions for unit energy dissipation	45
6.5	Particle emissions dependence on Disc Temperatures.	48
6.6	WLTC.....	54
7	Conclusion	60
	Discussion and Suggestion	62
	Bibliography	63
	List of Tables	66
	List of Figures	67
	Appendix	70

1 Introduction

Air quality is important for any life form to sustain on the planet earth. The quality of air can be influenced by both natural and man-made activities. Increase in economic and societal activities over the years have decreased the quality of air. There are about 400,000 premature deaths due to air pollution in the European region where the road transport has significant contribution to this burden [1]. Air pollution is a mixture of various gases such as carbon monoxide, sulphur dioxide, nitrogen oxides, ozone and combination of particles ranging from few nanometers to hundreds of micrometers. According to World Health Organization (WHO) , particles are one of the major pollutants in the air which have adverse effects on environment and human health [2].

Particulate matter (PM) is one of the major contributors to emissions from on road vehicles. It is classified into two categories namely exhaust and non-exhaust PM emission. Exhaust PM emissions are a result of incomplete combustion and lubricant volatilization whereas non-exhaust PM emissions are derived from wearing of brakes, tyres, clutch and resuspension of particles on the road due to traffic induced turbulence [3]. As the exhaust related PM emission is being monitored and controlled before leaving the tailpipe [4], the relative contribution of non-exhaust PM to the total particles emitted from the vehicle is increasing and there are no such legislative standards laid out as of now to monitor these emissions from non-exhaust sources and therefore will probably require regulation in the future [5]. Therefore, there is a strong motivation to investigate PM emissions from brakes.

1.1 Particulate Matter

Particulate matter (PM) is a very general term which is a mixture of solid, liquid or solid and liquid particles suspended in air. It is of complex mixture and can vary greatly in size, composition and the nature of formation [6]. They can be directly emitted from the

sources or indirectly from the gaseous pollutants already in air which turns into particulate matter. Therefore, it is grouped into primary and secondary particles.

Primary particles are emitted from sources such as road vehicles, heavy machineries, mining, construction and burning activities (e.g. burning of wood, forest fires etc.). Secondary particles are formed in the air due to the intermediate reactions of gases such as sulfates, nitrates and carbon containing reactive organic gases [7].

1.1.1 Particulate Matter Classification

Particles are broadly classified into fine and coarse particles based on their particle diameter (D_p). Usually $PM_{2.5}$ and PM_{10} (particles with aerodynamic diameter smaller than 2.5 or 10 micrometers, respectively) are monitored at the emission sources and in the ambient air [7]. Coarse particles are the particles between PM_{10} and $PM_{2.5}$ and PM_{10} refers to all the particles of size diameter below $10\mu m$. They are formed from the mechanical break-up of larger particles and settle down without much air travel. These include most visible forms of particles such as soil, dust from construction and mining operations etc.

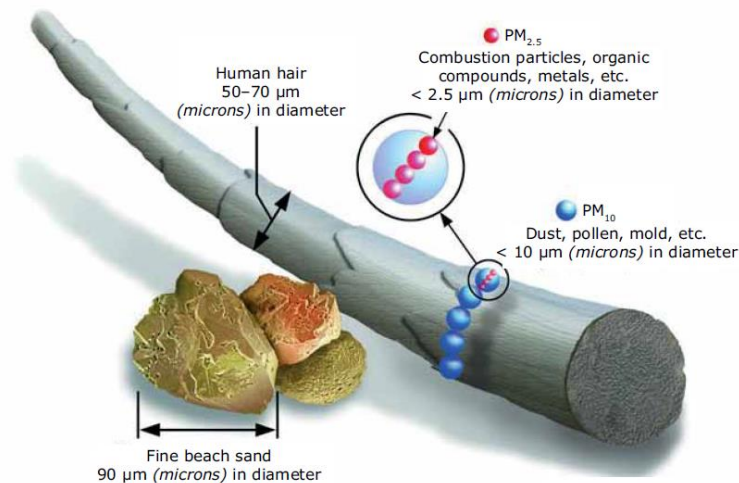


Figure 1.1 Illustration of $PM_{2.5}$ and PM_{10} [8]

Fine particles are the ones which fall between particle diameter of 0.1 μm - 2.5 μm . They are generated from primary sources such as combustion particles and formation of secondary particles which is due to condensation and coagulation [9]. Fine particles or PM_{2.5} are also known as respirable particles which can travel to the respiratory tract. The Ultra fine particles (UFPs) which has particle diameter less than 0.1 μm dominate the surface area of PM emissions but do not contribute majority to the PM mass concentration. UFPs are very unstable and grow into larger particles through coagulation and condensation. Due to their very small size, they penetrate greater into the lungs and mix with the blood stream [10].

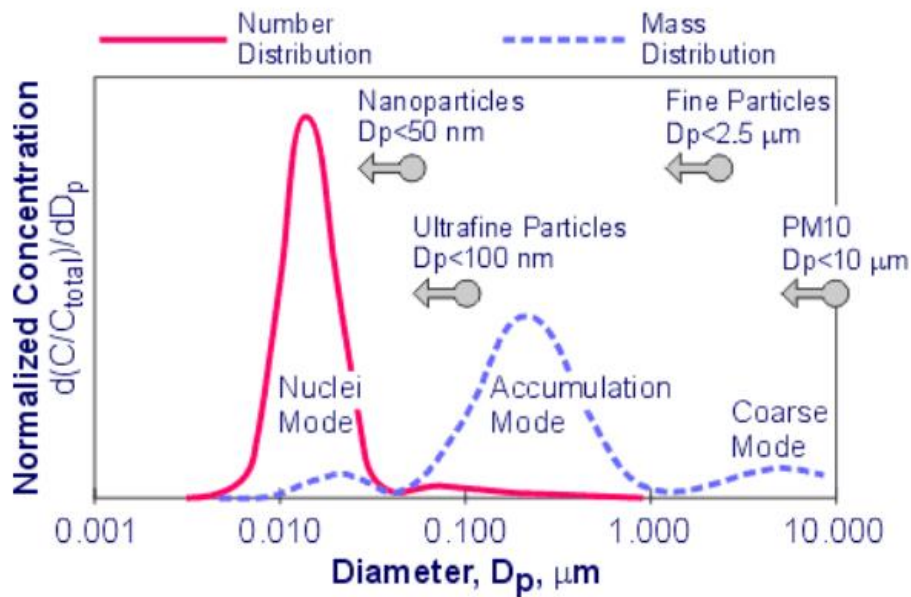


Figure 1.2 Size distribution of Particles [11]

1.1.2 Mechanism of Particle formation

Presence of gaseous precursors in the atmosphere is the most important aspect in particle formation due to the process called nucleation. The nucleation of gases molecules in the atmosphere contributes to the Ultra fine particulate matter. These UFPs have high particle number density and high thermal energies as a result these particles are suspended in air for longer periods of time and have shorter residence time. The rapid

growth in size of these particles to fine particulate matter proceeds either by condensation of other gases molecules on the particles or due to collision between the particles during random motion called coagulation gives rise to fine particulate matter [12].

The growth beyond fine particle region is moderate because of slower random motion of molecules which hinders coagulation rate. Particles being formed from the condensation of gases in the atmosphere tend to aggregate (this is called the accumulation mode) and are removed by subsequent rainout. Finally, the coarser particles which are above 2.5 μm in size sediment fast as they are relatively larger in size but very less in number and hence get removed by rainout [12]. The *figure 1.3* below shows the trimodal size distribution, showing the sources, the general size ranges and the removal mechanisms of particles.

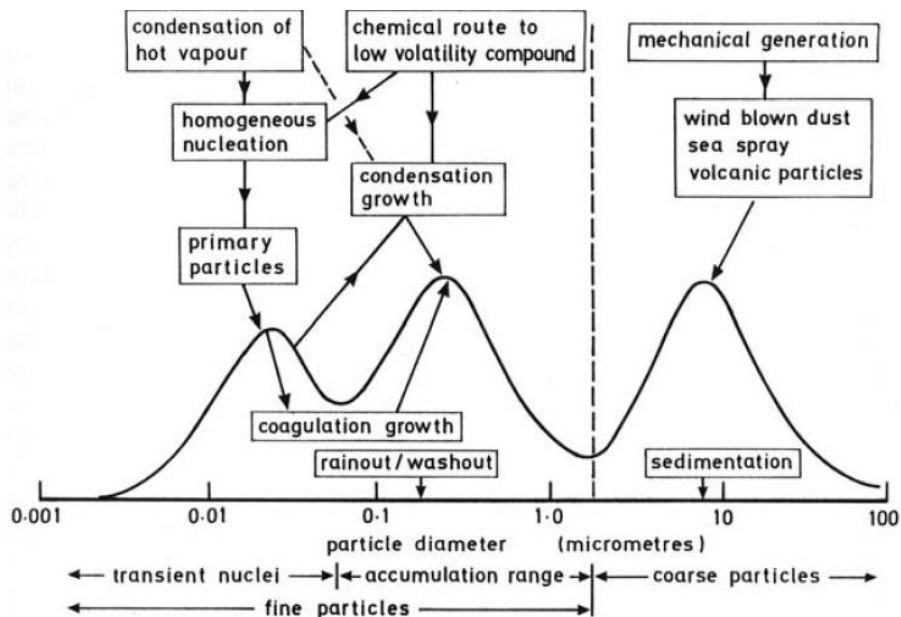


Figure 1.3 Formation of Particulate matter in atmosphere [12]

1.2 Effects of PM on human health and Environment

According to WHO, around 7 million people face premature death every year worldwide due to the exposure to fine particles in air [13]. Long-term exposure could also lead to various morbidities such as asthma, lung cancer, type 2 diabetes and loss of cognitive function. The mentioned illnesses are just the tip of the iceberg, because the various sources of PM generation and its profound impacts are still unclear [14]. The size of the PM influences the way it travels in the air and interacts with the human body. The smaller the particle size, the deeper it penetrates and deposits in human lungs as shown the in *Figure 1.4*. Mortality in cities is 15-20 % higher due to high levels of air pollution as compared to rural areas. The average life expectancy is estimated to be lower by 8.5 months in EU due to $PM_{2.5}$ exposure resulting from human activities [8].

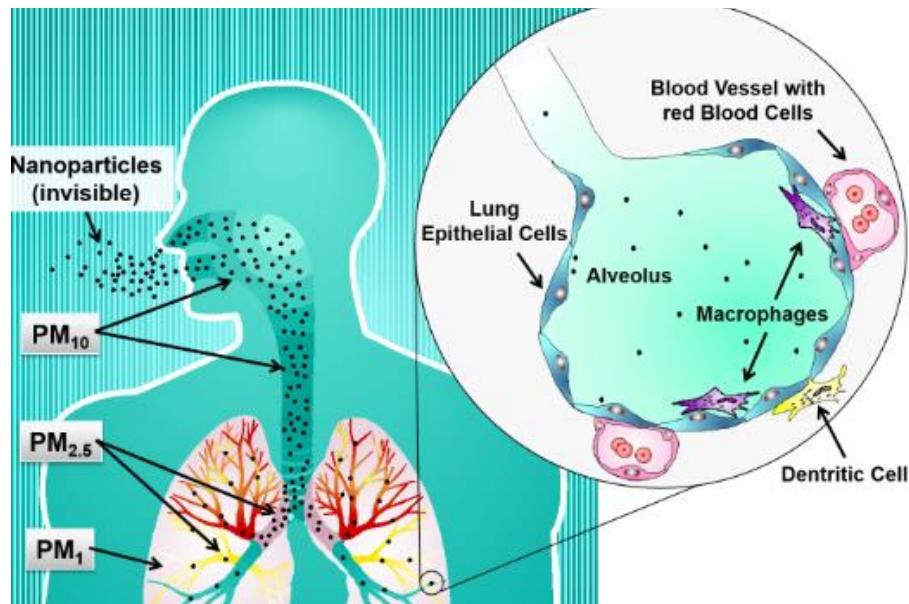


Figure 1.4 Possible Pathway of PM transport in human lungs [15]

The effects of particulate matter on environment is even more devastating. It contributes to global warming which makes the sustenance of bio-diversity difficult [16]. The effects of global warming are already being apparent in the form of rising sea levels, extinction of plant and animal species etc. [17]. Fine particles ($\leq 2.5\mu m$) are responsible

for the poor visibility in urban areas which can hamper road safety for the users. In addition to this, PM can corrode and soil the buildings which deteriorates the buildings life depending on the composition of the PM [8]. *Figure 1.5* shows the sector wise share of PM₁₀ and PM_{2.5} particle emissions. The contribution of road transport to particulate emissions is 10.7 % for PM₁₀ and 16 % for PM_{2.5} respectively [18].

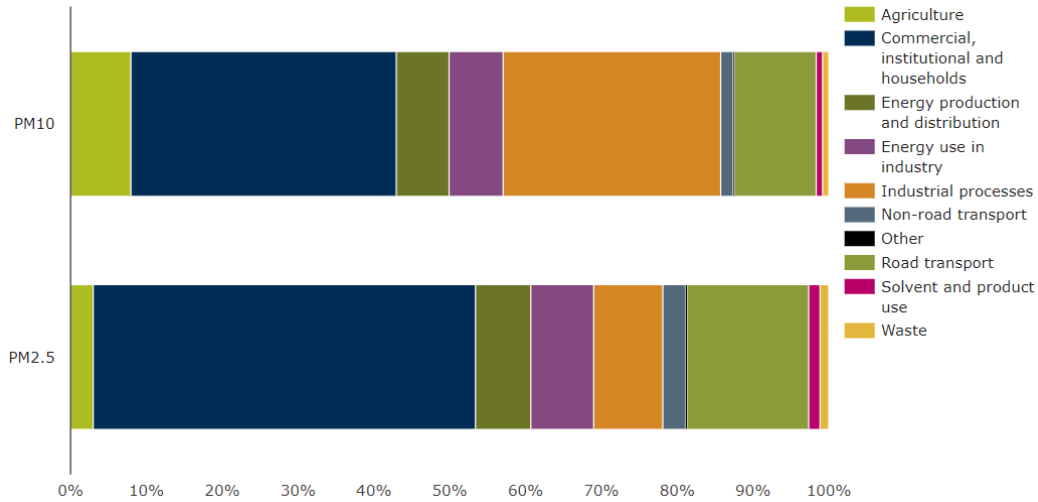


Figure 1.5 Sector share of PM_{2.5} and PM₁₀ emissions [18]

1.2.1 Ambient Air Quality

Air pollution is a major threat to the human health. Most of the areas in Europe still have poor quality of air despite of reduction in emissions and ambient concentrations. It is one of the biggest concerns for Europeans after climate change according to the European commission. Around 3000 air quality monitoring stations are setup in EEA-39 countries in order to assess concentrations of various pollutants in ambient air along with PM₁₀ and PM_{2.5} concentrations which is one the major pollutant. Legal limits of PM₁₀ and PM_{2.5} are set by ambient air quality directive of EU 2008/50 and are summarized in the table below [19].

Table 1.1 Air quality standards for protecting human health for PM10 and PM2.5 [19]

Pollutant	Averaging period	Legal Limit and concentration	Comments
PM ₁₀	1 day	50 µg/m ³	Not to be exceeded on more than 35 days/year
	Calendar year	40 µg/m ³	
PM _{2.5}	Calendar year	25 µg/m ³	

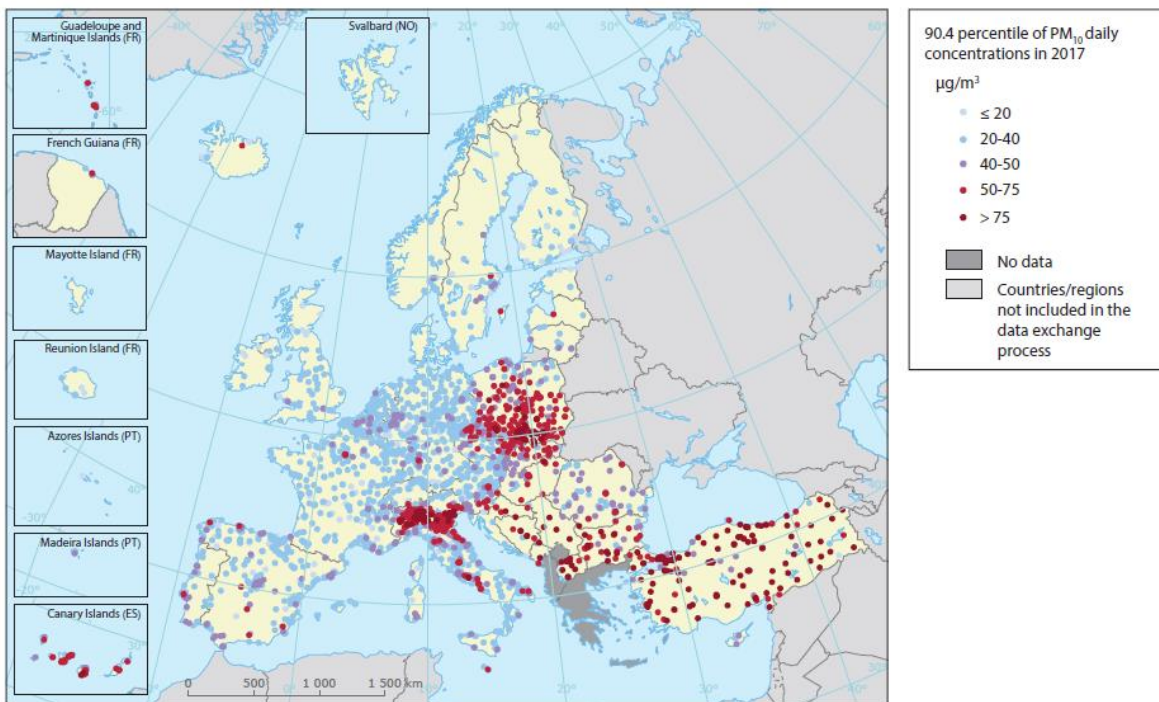


Figure 1.6 Observed daily mean concentration of PM10 [19]

Figure 1.4 shows the average daily concentration of PM₁₀ taken from 2886 stations. Only stations with 75 % of valid data have been considered. Stations marked in red and dark red exceed daily limit value which constitutes 17 member states. Moreover, 95 % of those stations are in urban (83%) and sub-urban (12%) areas. In 2017, concentrations above PM₁₀ daily limit value were recorded across 6 rural background stations in Czechia and with respect to PM_{2.5}, 1 rural station in Czechia registered above the prescribed annual limit [19].

1.3 Brake

Brakes assist the vehicle to slow down or bring it to complete stop i.e., kinetic energy of the vehicle is dissipated as heat energy. There are basically two brake configurations in use for passenger cars namely disc and drum setup. Most of the modern cars use disc brake at the front axle and disc/drum brake at the rear.

Majority of the passenger vehicles employ disc brake setup at the front which have to provide about 70% of the braking power. Disc brake setup performs better in extreme conditions as it is not sealed off from the ambient air and hence cools faster than drum brakes and thus maintaining higher brake effectiveness [20].

1.3.1 Brake mechanism

Disc and drum brake setup decelerate the vehicle with help of friction. Drum brake has curved shoes with linings on it which are forced against the inner surface of the rotating cylinder. On the other hand, the disc brake setup comprises of a rotor disc, caliper and brake pads. The caliper with the friction materials known as pads/linings surrounds the rotor as shown below in *figure 1.7*. The force on the piston pushes makes the caliper move towards the rotor during braking thereby slowing down the rotating disc and therefore the vehicle. The kinetic energy of the vehicle is dissipated as heat at the contact surface of the rotor and pad [21].

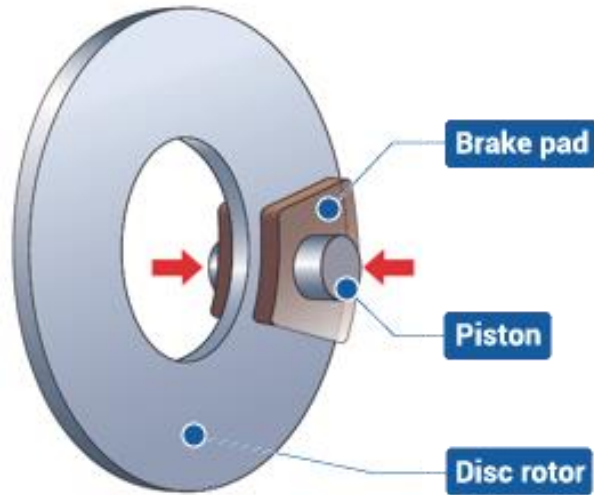


Figure 1.7 Disc brake working mechanism [22]

1.3.2 Brake emissions

Friction contact between rotor disc and brake pad during deceleration is one of the major sources of PM emissions from on road motor vehicles. Besides, some disc brake systems require low pressure contact of pads with rotor to have better braking performance by removing oxide layer but has the disadvantage of - particle release and increased fuel consumption [20]. Since majority of the braking is done by front brakes, they emit greater PM emissions and as a result the front linings must be replaced more frequently. The rate of the brake wear depends on the composition of the linings and the operating conditions of the brake which subsequently influences the chemical and physical properties of the emitted particles [23].

Braking is considered to be one of the major sources of non-exhaust traffic related particle emissions especially in urban areas and could contribute around 16-55 % by mass to total non-exhaust particulate emission [24]. One of the experiments conducted on brake dynamometer with different brake linings show that 86% of brake wear particle mass concentration was distributed in fine $PM_{2.5}$ and 63% in Ultrafine particulate matter in $PM_{0.1}$ (UFPs) region [25]. This can be due to the volatilization of the brake material which could condense in the air and therefore form fine particulate matter.

The exact composition of the individual components varies across the linings and its intended application. Moreover, in depth details of the composition are not fully disclosed by the manufacturers due to proprietary rights. So, in the broader view brake linings generally comprise of five major components [23]:-

- **Fibres:** Provide mechanical strength by reinforcement and accounts for 6-35 % of the brake lining mass. Fibres of carbon, glass, minerals are frequently used.
- **Abrasives:** Helps to increase friction and hinders built-up of heat transfer films which will reduce braking efficiency. Around 10% of lining mass is comprised of abrasives. Oxides of Al, Fe, Quartz are usually employed.
- **Lubricants:** It contributes 5-29 % of lining material and help in stabilizing frictional properties at high braking temperatures. Common materials used are graphite and metal sulphates.
- **Fillers:** They help in reducing manufacturing costs and improve manufacturability of the brake linings. Typical materials used are barite ($BaSO_4$) and mica and contribute 15-70% to lining.
- **Binders:** This component holds all the components together which is to retain the structural integrity of the lining. Phenolic resins are extensively used with variation of 20-40% depending on the required performance.

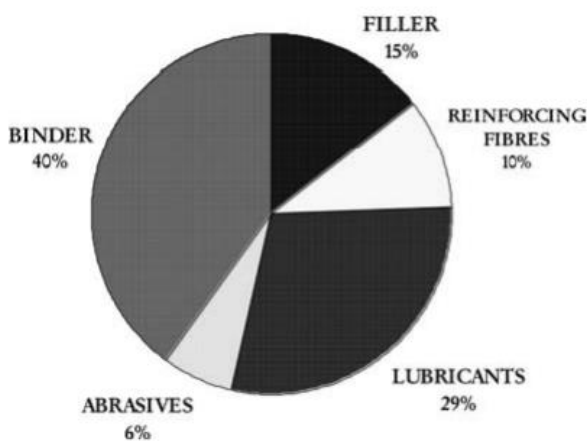


Figure 1.8 Typical Composition of brake pad [26]

2 Goal of the Thesis

The goal of the thesis is to analyze the data from brake wear particle measurement campaign comprising four types of brake pads with tests carried out on portions of standard test procedures ISO 26867, SAE J2522 and newly developed WLTC brake cycle performed on full scale Inertia brake dynamometer at Technical University of Ostrava and to evaluate:

- The particle emissions characteristics, which includes total number of particles and its size and mass distribution in different size bins considering braking intensity, friction surface temperatures, dissipated power and work.
- To evaluate and reconcile the measurements from instruments such as ELPI and EEPS and summarize the results.

3 Experimental Setup

The tests were carried out on a brake dynamometer with four different brake pads which are procured from local dealers based on the popularity and make for the vehicle model in this experiment. One set of pads were taken from an authorized vehicle dealer without any prior information about the actual manufacturer of the pad labelled as 'Original'. Remaining three sets of pads were selected based on a survey among local part dealers for the most popular aftermarket brake pads and labeled as 'Zimmerman', 'Ferodo' and 'ABE' according to their trade labels.

3.1 Brake Dynamometer

In order to test the brake pads, the most effective way to perform is to simulate the real braking conditions on a brake dynamometer. This is the closest way to represent real world braking scenarios and test procedures under controlled conditions. For this reason, full scale brake dynamometer was chosen for the testing procedures. The experiment was carried for a week starting from 8.10.2019 to 15.10.2019 at Technical University of Ostrava. Front brake assembly with original caliper and a typical rotor of one of the most popular passenger cars (according to vehicle registrations) in Czech Republic was coupled to a full scale brake dynamometer as shown in *Figure 3.1*. The rotor is coupled by a rotating shaft to an asynchronous electric motor and a flywheel. The assembly is accelerated to the desired speed by the motor. When prescribed conditions are reached such as temperature, hydraulic pressure in the brake lines are regulated via actuator to match the target brake line pressure or deceleration rate. The rotor is coupled to the flywheel simulating vehicle translational and rotational inertia corresponding to approximately 37.5% of the vehicle equivalent test mass (75% of brake effect on front and 25% on rear wheels). The desired equivalent test mass was 1840 kg for the entire vehicle, corresponding to the gross vehicle weight (GVW), and 690 kg for the tested wheel. The actual test mass was 753.5 kg, corresponding, at 308 mm wheel rolling radius,

to a mass momentum of inertia of 71.5 kg-m². Thermocouple inserted in a hole drilled radially into the rotor measured the temperature of the rotor.



Figure 3.1 Brake Dynamometer used for the experiment [27]

The rotor and the brake assembly are housed in an airtight enclosure as shown in the *Figure 3.1*. through which air was circulated by fans a flow rate of 2400 m³/h to provide cooling for the brake assembly and to scavenge fumes and smaller brake wear debris from the enclosure. Part of the outlet duct was replaced by a 30 cm diameter, approximately 5 m long pipe, serving as a dilution tunnel for particulate matter sampling. The sampling port was installed approximately 3.5 m from the last bend and 5.5 m from the brake assembly, corresponding to a residence time (for the particles to travel to the sampling point) of approximately 0.75 seconds.

3.2 Instruments used in the experiment

Online Particle size classifiers are employed at the test facility to measure particles emitted from the brake assembly during and after the braking event. Dekati Electrical Low-Pressure Impactor (ELPI+) and TSI Engine exhaust particulate size spectrometer (EEPS) are the ones used in this experiment to measure PM.

3.2.1 Electrical low-pressure impactor (ELPI+)

ELPI+ is used to measure real time particle size and concentration in the size range of 6nm-10 μ m. The instrument classifies particles into 14 size classes depending on the aerodynamic size of the particle (D_p). The particles are charged with the corona charger before entering series of cascade impactors. The principle of inertia makes the particles to settle down on the respective impactor stages [28].

The particles larger than certain aerodynamic size get collected on the upper impactor stages and smaller ones travel down to the lower stages and get settled. This is due to of particles larger than certain aerodynamic diameter resist to take a turn and settle down on the impactor while smaller particles remain in the flow. The electrometers attached to the corresponding impactor stages detect the charge carried by the particles [28].

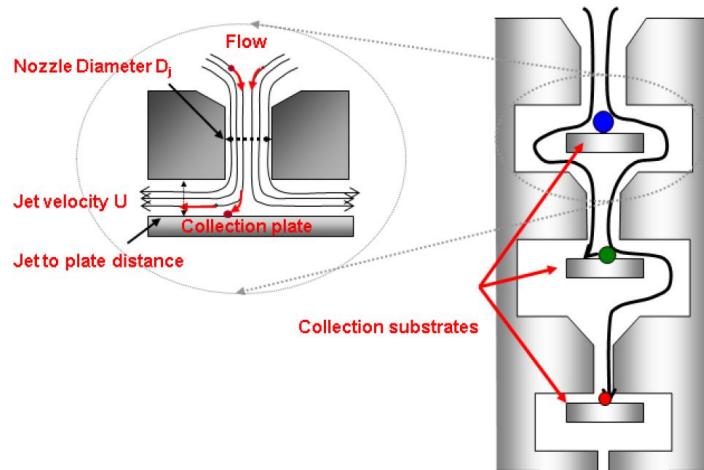


Figure 3.2 Schematic representation of ELPI [28]

3.2.2 Engine Exhaust Particle Sizer (EEPS)

EEPS is fast response and high-resolution particle measurement instrument having capability of measuring the particles of size in the range 5.6-560nm. The particles entering

the instrument are positively charged to a predictable level at the inlet with the help of corona charger and are transported downstream with help of filtered sheath air [29].

The classification of particle is based on differential electrical mobility. When the charged particles enter the column above the central electrode as shown in Figure 1.6, the particles are deflected radially outward and collected on the electrically isolated electrodes. The particles with high electrical mobility are deflected to the electrode at the top and the with lower mobility comes further to the downstream. The electrodes are connected to a sensitive charge amplifier known as electrometer [29].

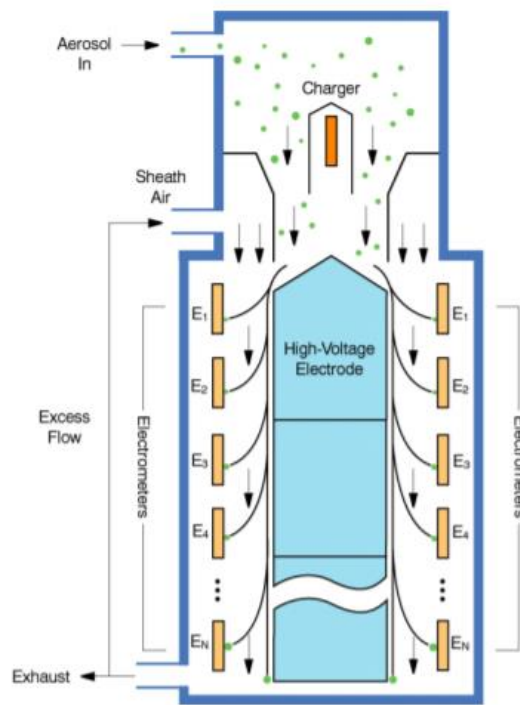


Figure 3.3 Schematic diagram of EEPS [29]

4 Brake Wear Test Procedures

The wear and durability of the braking system is assessed with the help of certain standardized test procedures to estimate the wear life of the friction pair at the design stage. This is carried out using some laboratory based methods rather than vehicle based due to cost and time constraints. Testing of modern composite friction materials consists of a series of repetitive braking scenarios from a set speed and certain initial temperature range. This approach serves as the basis for comparison of different friction materials under similar conditions. Therefore, to assess the wear of the four pads, some sections from standardized ISO 26867 and SAE J2522 procedures were selected. Standardized brake wear testing procedures typically comprise a range of extreme events, including a simulation of brake fading during prolonged hill descent and during repeated hard stops from very high speeds. These tests are intended to assess the brake performance during most extreme conditions rarely encountered during ordinary operation. To represent, as much as possible, ordinary operation, sections without extreme events were selected from two standard brake test procedures. The following are the standardized test procedures employed by automotive industry to assess brake and its performance on vehicles.

- Federal Motor Vehicle Safety Standards (FMVSS) and the National Highway Traffic Safety Administration (NHTSA) Regulations.
- Standards from Society of Automotive Engineers (SAE).
- International Standards from the International Organization for Standardization (ISO).
- Regulations from the United Nations Economic Commission for Europe (UNECE).

4.1 ISO 26867

The test procedure is to assess the influence of braking parameters such as pressure, temperature and linear speed on the friction co-efficient for a given friction

material mated to a given disc or drum. It is intended to compare friction materials under the same testing conditions which are important for brake friction material development [30]. The test cycle has a total of 167 braking cycles grouped into 24 sections out of which portions of 5 sections consisting of 72 cycles altogether were chosen for the experiment. All the four brake pads are subjected to the same procedure. Each brake cycle consists of braking the disc to the set speed, cooling of the disc and accelerating to the desired set speed for the next braking event according to the section requirements. *Table 4.1* shows the six sections selected: degreening (ISO 26867 section 1) and bedding (ISO 26867 section 2), together referred to as the degreening phase, and for the main test phase, ISO characteristic value sections 3, 5 and 8 were carried out. The following tables summarizes the sections with the cycle details: -

Table 4.1 Sections of ISO 26867 testing procedure used in the test

ISO characteristic section (#)	Initial speed (kph)	Final speed (kph)	Initial Disc Temp (°C)	Average Pressure (Bar)	Repetitions
A (ISO 1)	80	30	150	30	10
B (ISO 2)	80	30	200	15-50	32
C (ISO 3)	80	30	150	30	6
D (ISO 5)	80	30	150	30	6
E (ISO 8)	80	30	150	30	18

4.2 SAE J2522

This procedure is also known as “Dynamometer Global Brake Effectiveness” which evaluates the friction material effectiveness based on the braking parameters such as speed, temperature of the disc and pressure for motor vehicles equipped with hydraulic brakes. It was developed in Europe in co-operation with vehicle, brake and friction material manufacturers. This is also known as AK Master test procedure. The main purpose is to assess and compare the friction materials performance under the same testing conditions as closely as possible. Friction behavior such as speed sensitivity, fade

resistance and friction recovery are evaluated. It has total of 10 sections and 404 brake cycles in total out of which portions of 6 sections comprising of 35 cycles were reproduced on the dynamometer [31]. SAE sections of characteristic value 4.1, 4.2, 4.3, 6, 7 and 11 are summarized in the *table 4.2* below: -

Table 4.2 Sections of SAE J2522 testing procedure used in the test

SAE characteristic section (#)	Initial speed (kph)	Final speed (kph)	Initial Disc Temp (°C)	Average Pressure (Bar)	Number of brake events
F (SAE 4.1)	40	5	100	10, 20, ,80	8
G (SAE 4.2)	80	40	100	10, 20, ,80	8
H (SAE 4.3)	120	80	100	10, 20, ,80	8
I (SAE 6)	40	5	40	30	1
J (SAE 7)	100	5	50	50	1
J (SAE 7)	180	100	50	60	1
K (SAE 11)	80	30	100	10, 20, ,80	8

4.3 Sequence of test procedure

The test carried out on the four pads followed the characteristic section numbers of ISO and SAE test procedures summarized in the *table 4.1* and *table 4.2*. The test procedures carried out are divided into degreening and testing phase. Sections 1 and 2 of ISO together is called degreening phase and this processes is required to make sure that the system with new pads and rotors are in uniform contact and resins from the pad material are removed at the surface contact of the disc and pad [32]. The remaining sections of ISO and SAE are grouped into testing phase. Firstly, the test procedure was started with ISO 1 section (parameters described in *table 4.1*) and was repeated for 10 consecutive times. Then, the pads were subjected to ISO 2 section with initial disc temperature of 200 °C and average pressure varying between 15-50 bar. This section is also called bedding procedure.

The testing phase starts with section ISO 3 with initial temperature of 150 °C and average pressure of 30 bar repeated consecutively for 6 times. The next 3 sections carried

out were SAE 4.1, 4.2 and 4.3 with 8 braking events in each section and initial disc temperature at 100 °C throughout these sections. The average pressure was incremented by 10 bar after each braking event and goes all the way up to 80 bar. Thereafter, ISO 5 section was carried out with same parameters as section ISO 3 and repeated for 6 consecutive times. Following this, sections of SAE 6 and 7 were performed for one time each. The next section was section ISO 8 with same braking parameters as ISO 5 and ISO 3 but now repeated for 18 consecutive times. The testing phase ended with SAE 11 section with initial disc temperature of 100 C repeated for 8 consecutive times incrementing average pressure in steps of 10 bar after each braking event and reaching up to 80 bar. *The sections of ISO and SAE are labelled in alphabets for representative purposes in the results chapter and has no significance with test run sequence.*

4.4 WLTC Cycle (Novel Test Cycle)

A novel braking cycle is developed aiming towards reflecting real world braking patterns and commonly accepted methodology for brake wear particles sampling and measurement. The cycle is developed based on the WLTP reference database which includes driving data from five different world regions with a total driving distance of 740,000 km. The Novel cycle (referred to as WLTC) has 303 stops with net duration of approximately 4.30 h for a distance 192 km with maximum braking speed of 132.5 km/h. The cycle is divided into 10 segments and the soak time is adjusted such that the starting temperature of the disc is below 35 °C before start of each segment [33].

In addition to the above four pads, another set of Zimmermann brake pads labelled 'Zimmermann V' was subjected to a milder degreening (64 stops, initial rotor temperature of 150° C, initial speed 80 km/h, release speed 30 km/h, variable brake pressure), representing a compromise between bedding procedures prescribed in ISO 26867 section 2 (32 stops at 200 °C initial rotor temperature) .The sections 3,5,8 of ISO are also different with lower initial rotor temperature (30 stops at 100 °C initial rotor temperature). This set was subjected to the above described test and in addition to this, three repeats of the newly developed WLTC brake testing procedure were carried on this

brake pad to check for consistency in PM emission. The following describes the newly developed brake WLTC test cycle. *Figure 4.2* is the graphical representation of the proposed WLTC Brake Cycle.

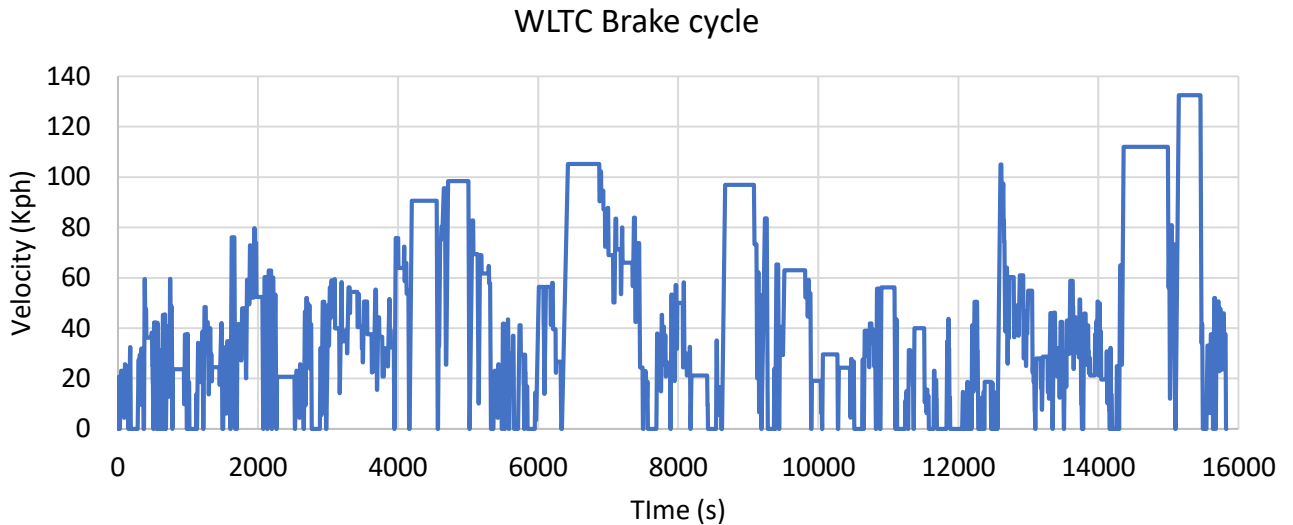


Figure 4.1 Velocity-time schedule of WLTC Brake cycle [33]

4.5 Comparison of Cycles

The selected segments of the ISO 26867 and SAE J2522 test procedures are compared with brake WLTC as shown in the *figure 4.2* and *figure 4.3*. These test cycles have high decelerations and high brake speeds compared to the brake WLTC cycle. It is clear from the *figure 4.2* that majority of the deceleration in WLTC are less than 1.5 m/s^2 whereas in the Standardized test procedures the decelerations are much higher. The similar trend follows even with the initial velocities. The test cycles operate at higher initial brake speeds and hence larger amount of energy is dissipated through brakes and reach higher final disc temperatures. The case with WLTC is different as it is derived from the real-world driving data and is intended for road driving, most of the initial brake speeds are below 75 kph whereas the test cycles are performed at the speeds of 80kph and above.

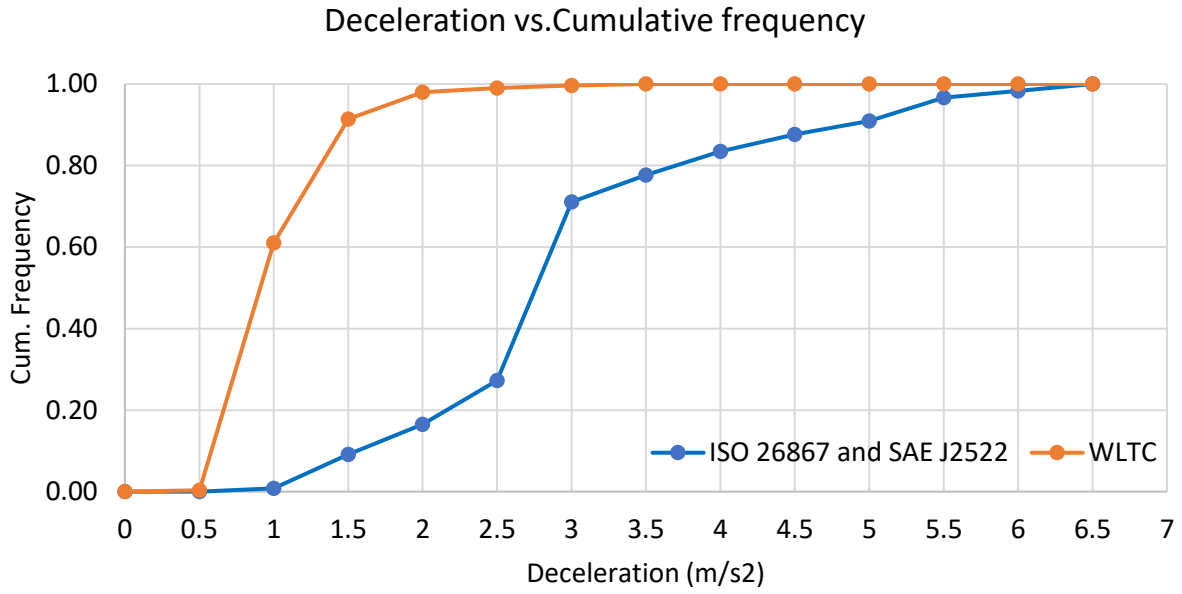


Figure 4.2 Cumulative frequency distribution of selected sections of ISO and SAE with regards to deceleration

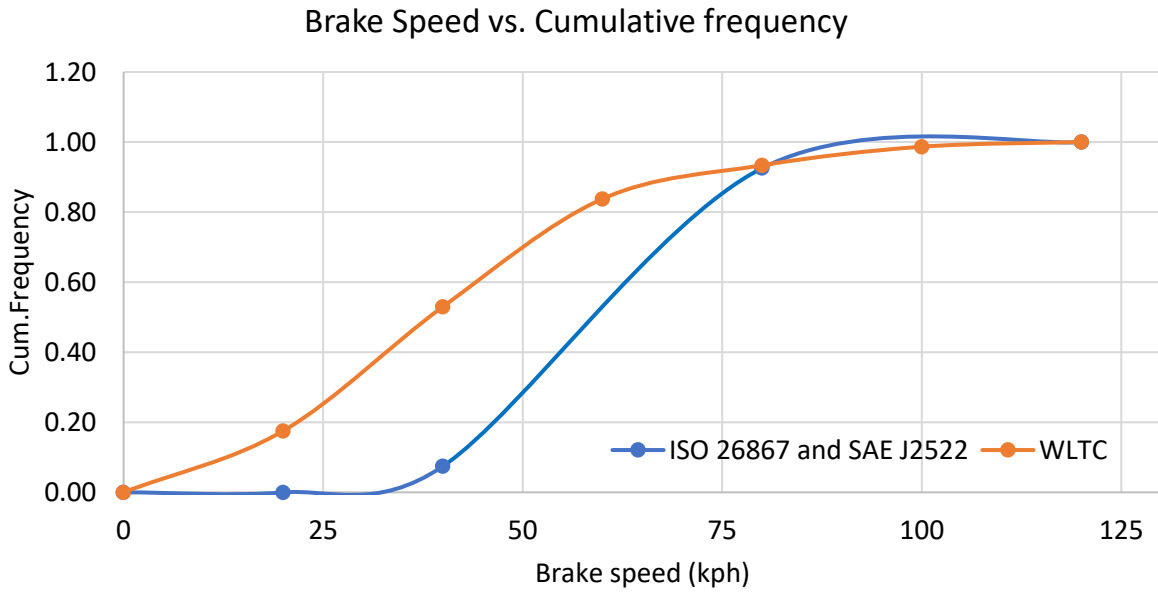


Figure 4.3 Cumulative frequency distribution of selected sections of ISO and SAE with regards to initial velocity

5 Data Analysis

The above-mentioned test procedures are performed, and the responses recorded by the instruments such as ELPI and EEPS are further analyzed to extract the useful data. Every response recorded by the instrument has two components namely useful signal and unwanted noise [34]. The main is to remove the noise and calculate the useful signal from the series of braking events.

5.1 Instrument Signal and Noise

The strength of the measured signal should be distinguishable from the noise which is recorded along with the useful response. So, to quantify this, Signal to Noise ratio (SNR) of the instrument is calculated to describe the performance of the instrument. The source of noise could be from within the instruments or from the influence of surrounding environment [35].

$$\text{Signal to Noise ratio (SNR)} = \frac{\mu}{\sigma}$$

Where, μ = Mean of the Signal

σ = Standard deviation of the Noises

Signal (μ) is obtained from the mean of the signal by subtracting the mean background value whereas standard deviation (σ) is calculated from the instrument when it is kept running before measuring any signal [34]. *Figure 5.1* shows the response of EEPS for series of brake events. It can be seen clearly in *figure 5.2* that the response obtained from the instrument has noise with the useful signal which is eliminated in the later data processing.

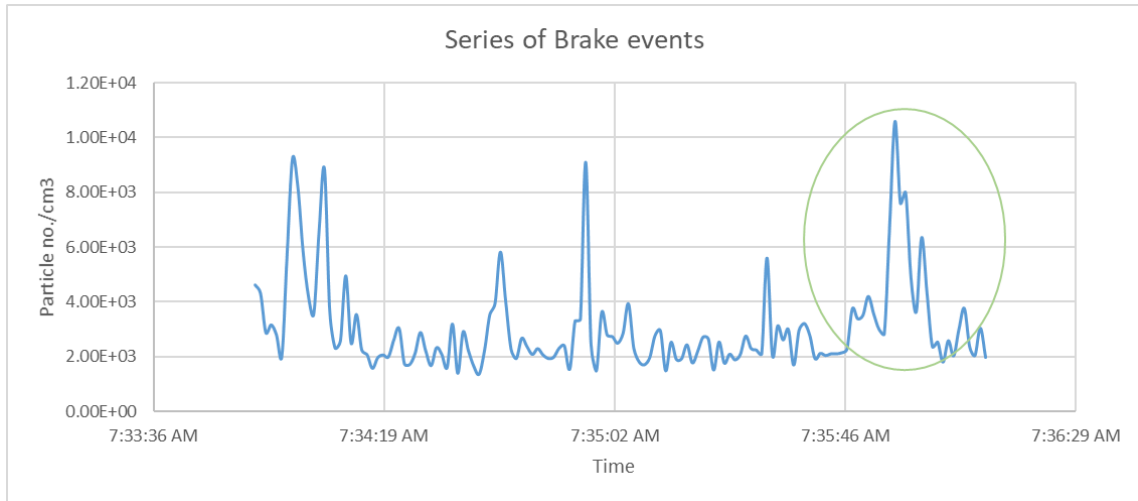


Figure 5.1 Showing response of EEPS for series of brake events

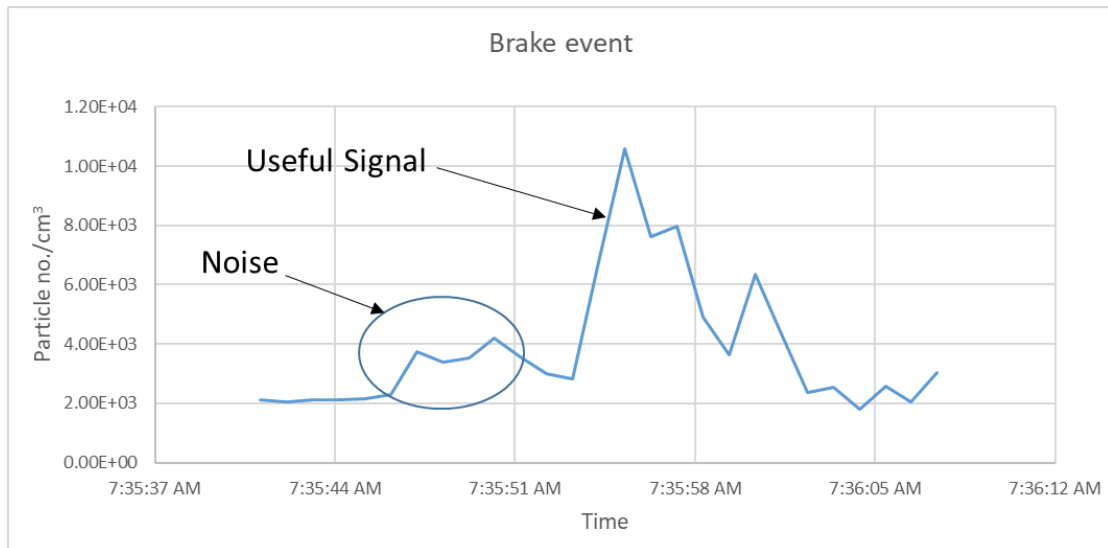


Figure 5.2 Enlarged view of a brake event showing Signal and Noise

5.2 Detection limit

The lowest possible concentration that the instrument can detect from the given concentration sample distinguishable from the noise. Detection limit specified by the manufacturers may not be the same always as it varies time and different operating conditions. The measuring instrument produces certain responses even without exposure to the sample known as background noise. These noises add up to the actual signal in real

measurement which exaggerates the sample response [35]. Therefore, detection limit is setup considering 2 types of errors. Type 1 decision error is also called false positive error which detects the concentration even though it is not present in the sample whereas false negative error called as type 2 error which does not take the concentration response despite presence in the sample. Considering this, which leads to uncertainty in the measurement the detection limit can be given as into detect the actual response of the instrument by calculating the Standard deviation of the background noise. Detection limit is typically given as a multiple of 3.3 times of the standard deviation of instrument noise [36],

$$\text{Detection limit} = \text{Standard deviation} \times 3.3$$

Where the Standard deviation is calculated from the background values without any sample concentration with certain confidence level. *Figure 5.3* shows the series of braking events performed on Original pad and data recorded by EEPS.

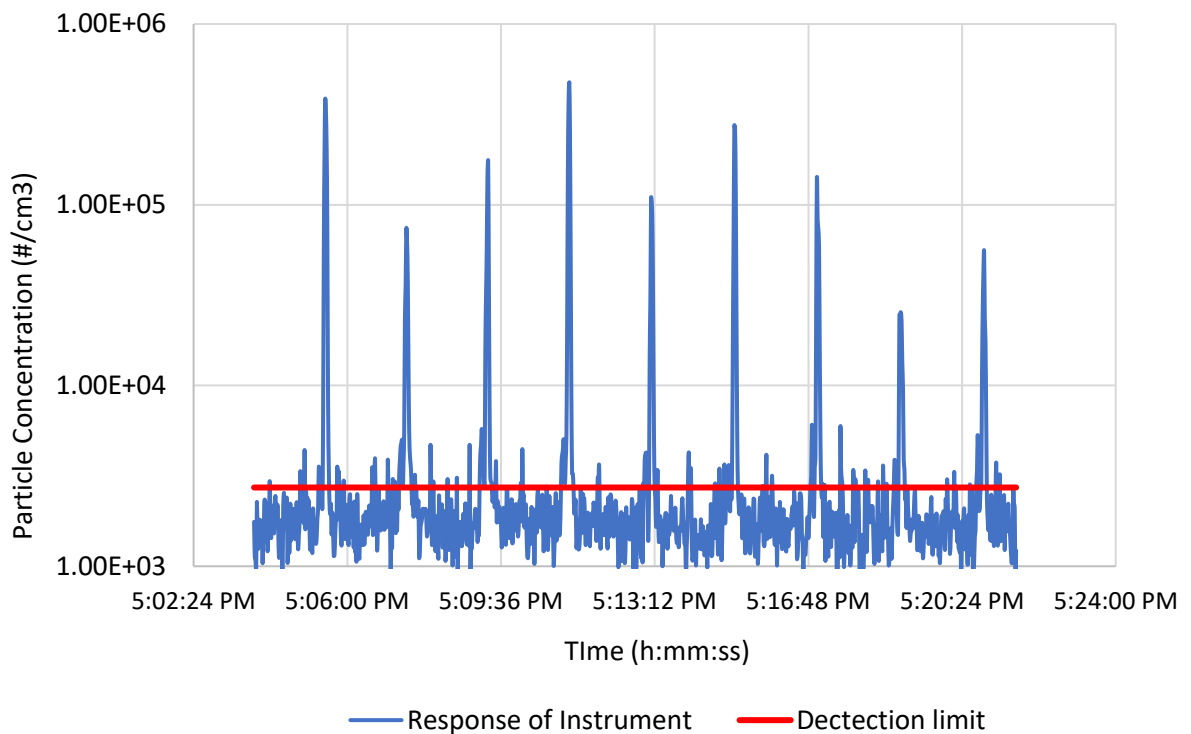


Figure 5.3 Peak areas above detection limit considered for analysis

5.3 Baseline and Peak Calculation

As discussed before, the response recorded by the instrument is a combination of both signal and noise and as a result there is uncertainty of the recorded response for the corresponding brake event. So, to reduce the measurement uncertainty the noise is minimized by subtracting the baseline value from total response of the event as shown in the *Figure 5.3*.

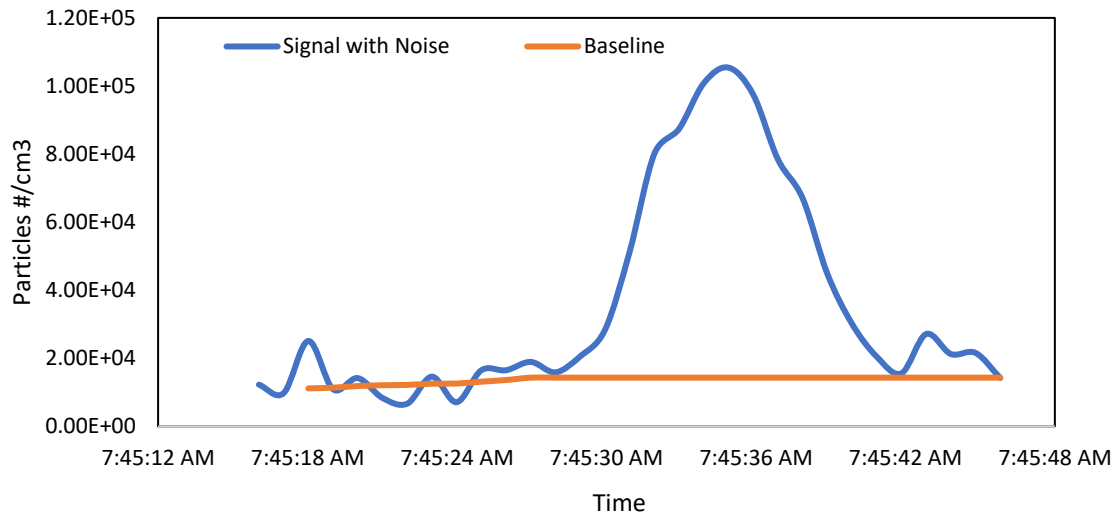


Figure 5.4 Baseline for the Instrument response

The procedure employed to create the baseline is by averaging the values for interval of 15 values just before the event and subtracting the baseline value from the Signal gives the useful signal as shown in Figure 5.4. The peak is integrated over the time to get the value of the useful response. The same procedure is followed for each and every brake event and for both the instruments ELPI and EEPS. The net concentration is obtained by: -

$$\text{Net concentration} = \text{Instrument response} - \text{Baseline (averaged value before the event)}$$

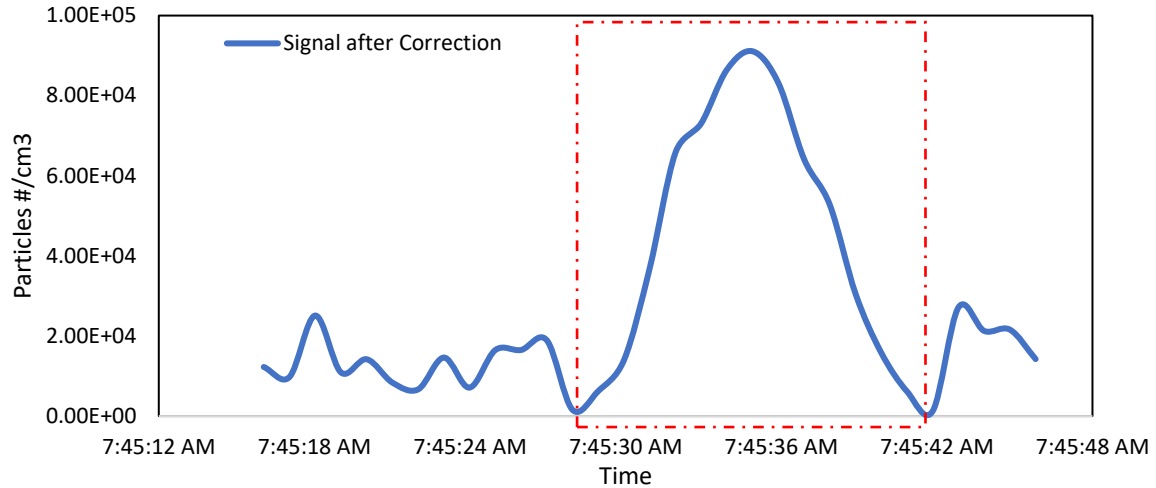


Figure 5.5 Signal after baseline correction

5.4 Time Synchronization between Instruments

The response recorded by the instruments for the corresponding brake event could be delayed sometimes due to various factors such as response time of respective instruments and length of sampling line. The timing of the brake event is recorded and is taken as a reference to check for the change in current/concentration values recorded in the instrument data sheets for the same time. It is observed that the instrument recorded the signal after 50 seconds of the event. So, both instruments had to be synchronized with braking time and then perform the analysis. This synchronizing is done to make sure that the responses recorded by the instruments are in line with the braking events performed on the dynamometer and measured value corresponds to the respective braking event.

Synchronizing of time between ELPI and EEPS

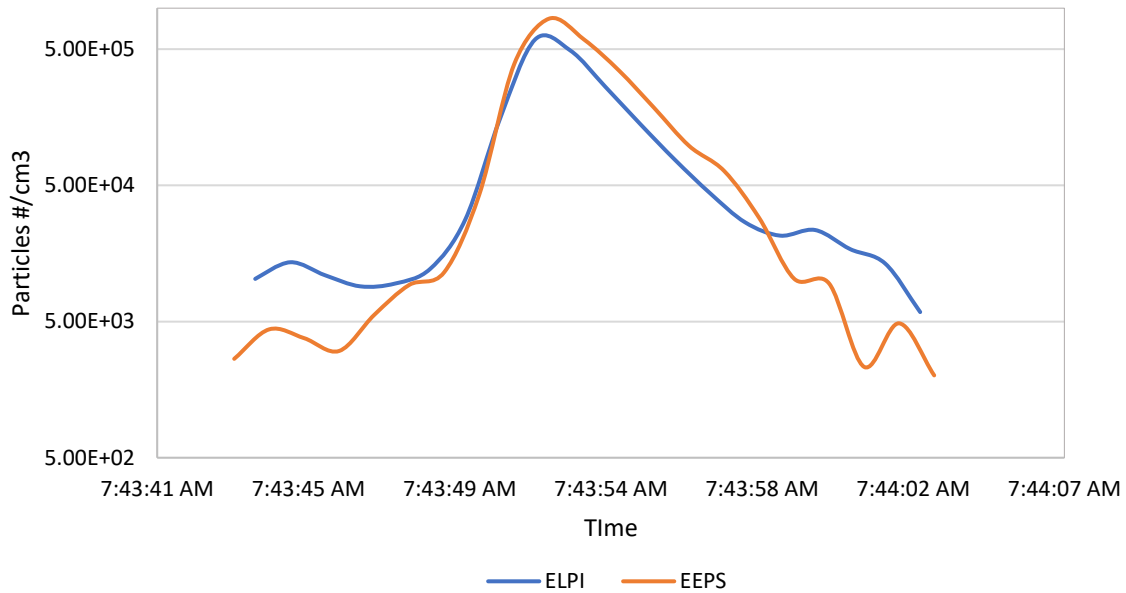


Figure 5.6 Time Synchronizing between ELPI and EEPS

5.5 Energy and Power dissipation

The kinetic energy of the vehicle must be dissipated through the friction brakes to slow down the vehicle or bring it to a complete stop. For example, a car of mass 1500 kg travelling at speed of 116 kph has to dissipate 735 kJ of energy through the braking system without considering any rolling and aerodynamic resistance losses [37]. In the experiment carried out, wheel load of 753.5 kg on left front wheel which translates to an equivalent mass moment inertia to 71.51 kg-m². The Inertia and kinetic energy can be calculated as follows: -

$$\text{Mass moment of Inertia } (I) = M \times r_{dyn}^2 \text{ (kg-m}^2\text{)}$$

$$\text{Kinetic Energy} = \frac{1}{2} * I * (\omega_{final}^2 - \omega_{initial}^2) \text{ (J)}$$

Where, I = Moment of Inertia (kg-m²)

ω = Rotation speed (rad/s)

M = Wheel Mass (kg)

r_{dyn} = dynamic wheel radius (m)

The time required to slow or stop the rotor from set speed is obtained from the test bench and hence the power can be calculated. Power is defined as the rate of doing work which means the rate at which the kinetic energy of the rotor is dissipated.

$$\text{Average power dissipated} = \frac{\text{Kinetic Energy}}{\text{Stop time}} (W)$$

5.6 Particle Size and Mass Distribution

Size of the particle is defined by its diameter known as particle diameter. Particles in a unit volume of sample can be classified into monodisperse and polydisperse depending upon their size ranges. Monodisperse particles have uniform size throughout and can only be produced under certain controlled laboratory conditions. On the other hand, polydisperse have particles with wide size ranges and the aerosol particles in the atmosphere are polydisperse in nature. Particles emitted from exhaust and non-exhaust sources are polydisperse in nature and its physical properties are strongly dependent on the size of the particle. Therefore, it is important to classify these size distributions by statistical means. For this, the entire size range is divided into series of successive size intervals and number of particles in each interval are determined. The size of each interval is called the bin width which varies with the instrument and its settings. Size bin is defined by the particle midpoint diameter (D_p) [38].

The particles emitted from brake fall into the category of polydisperse and therefore Particle Size Distribution is determined from particle number concentrations in respective size bins of the measuring instrument. *Figure 5.7* shows the graphical representation of the particles grouped in the respective size bins in EEPS. The concentration is plotted over the mid-point diameters (D_p) of the particles. As the distribution is skewed towards left, log scale is used on x-axis to approximate normal

distribution. Lognormal distributions are used if the difference between the highest and lowest range is about 10 or more.

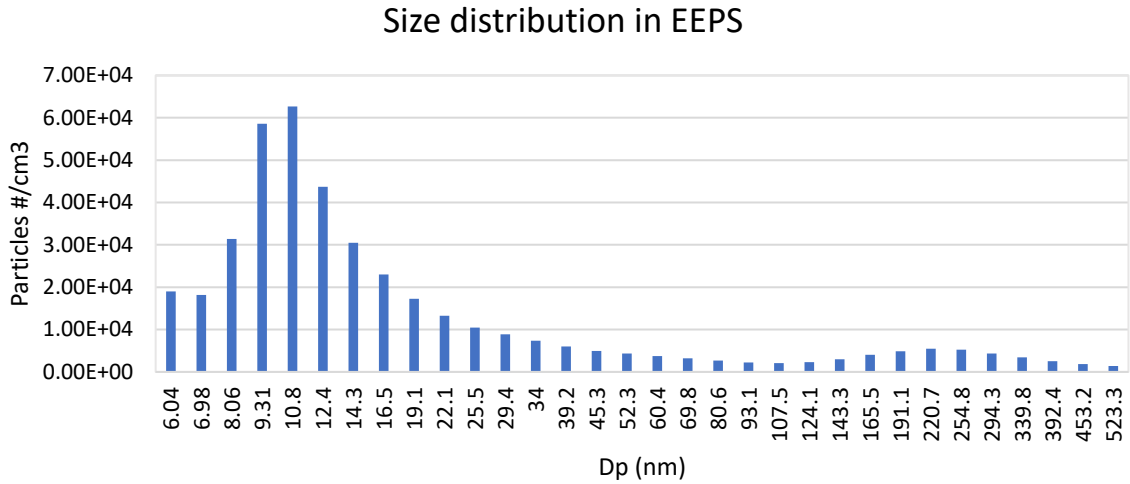


Figure 5.7 Particle size distribution (EEPS)

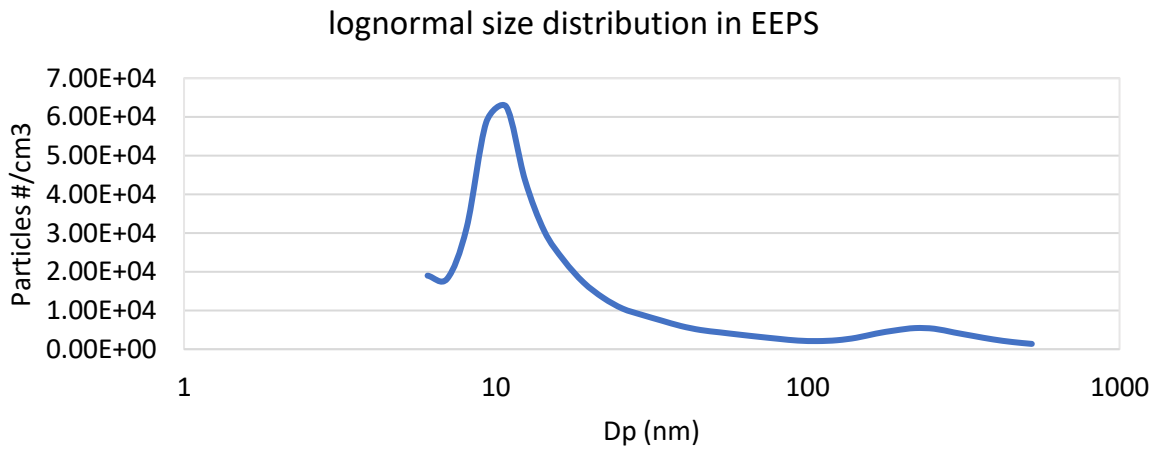


Figure 5.8 Lognormal particle size distribution (EEPS)

For comparing both the instruments such as ELPI and EEPS, the concentrations in respective bins must be normalized. Hence $dN/d\log D_p$ is used where dN is the number concentration in the respective size bin and $d\log D_p$ (log base 10) is the difference in size range of the bin [39]. The bin designations of ELPI and EEPS are given in the Appendix.

$$\frac{dN}{d \log D_p} = \frac{dN}{\log_{10} D_{p,u} - \log_{10} D_{p,l}}$$

Where, dN = particle concentration in the bin
 D_p = midpoint diameter of particle
 $D_{p,u}$ = upper channel diameter
 $D_{p,l}$ = lower channel diameter

Physical properties of particle such as number, mass, surface area and volume are described in terms of n^{th} moment of size distribution $(D_p)^n$. The properties of particles are proportional to n^{th} moment of particle diameter D_p such as number $(D_p)^0$, length $(D_p)^1$, Surface area $(D_p)^2$ and Volume $(D_p)^3$. These properties are calculated by knowing the number distributions in the size bins [38].

From the size distribution on ELPI and EEPS in *figure 5.9* and *figure 5.10* below from the same braking event, it is seen that ELPI has a greater number of particles compared to the EEPS in the respective bin sizes but the underlying fact is that the width of the bins of EEPS and ELPI are different with varying size resolution. The details of the bin sizes of ELPI and EEPS are given in the Appendix. Hence to avoid this confusion and misinterpretation, size distribution is normalized.

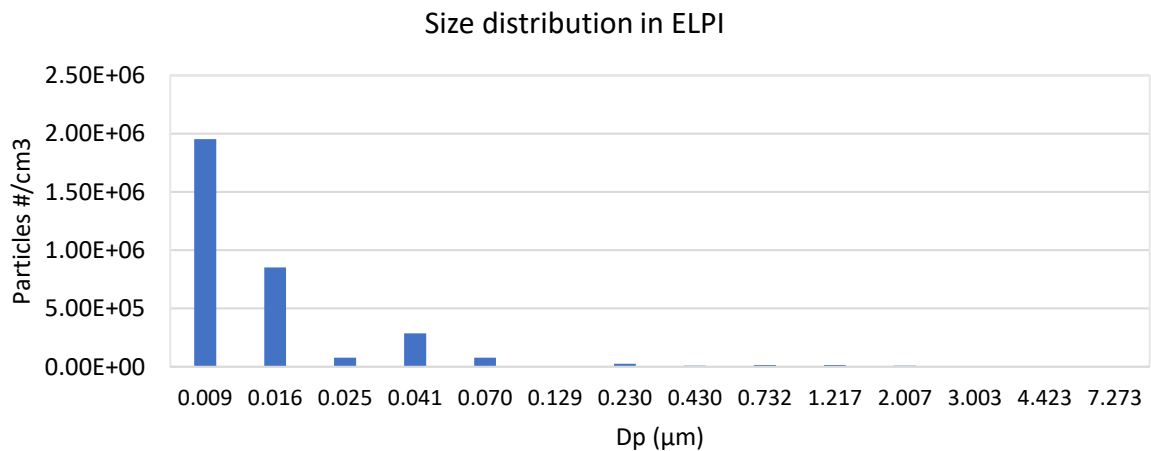


Figure 5.9 Particle size distribution in ELPI

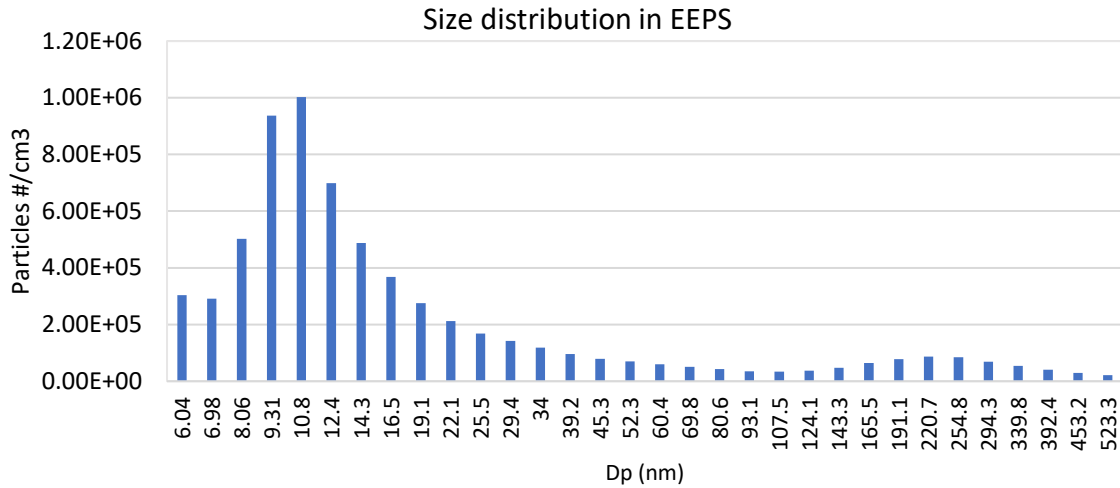


Figure 5.10 Particle size distribution in EEPS

Figure 5.11 and figure 5.12 shows the normalized particle size and mass distribution of a brake event with Original pad. Initial and final temperature of the disc are 100 °C and 200 °C with initial brake speed of 120 kph and final release speed of 80 kph with average pressure of 80 bar in the brake line are the parameters of the braking event. The differences in the peak concentrations of the EEPS and ELPI in figure 5.11 could be attributed to the measuring range and resolution of the instrument and its operating principle. EEPS classifies particles based on the electrical mobility whereas ELPI classifies particles based on aerodynamic particle diameter.

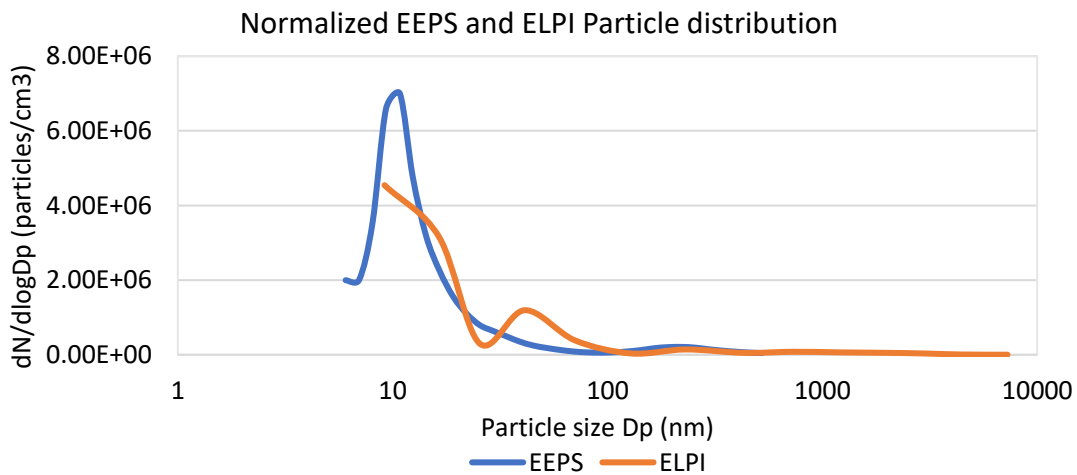


Figure 5.11 Comparison of Normalized particle size distribution in EEPS and ELPI

5.6.1 Integrated Particle Size Distribution method (IPSD)

This method estimates Particulate mass by Particle number concentrations which are classified based on the particle diameter D_p . Firstly, the number weighted particles in the size bins are converted into volume weighted size distribution by assuming the particle as perfect sphere and then multiplying it with the corresponding effective particle size dependent densities (ρ_{eff}) to get the mass distribution as given in the formula below [40]. Since the composition and morphology of the particles emitted from brakes are complex, the effective density (ρ_{eff}) of the particle is assumed to be 1 g/cm³ throughout the bin sizes. The distribution of mass can be calculated by the following equation [39]: -

$$\text{Volume of sphere} = \frac{1}{6} * \pi * D_{p,i}^3$$

$$M_{IPSD} = \sum_i \rho_{eff} * \frac{\pi}{6} * D_{p,i}^3 * n_i$$

Where, i = Index of the particle size range

ρ_{eff} = effective particle density (g/cm³)

$D_{p,i}$ = particle midpoint diameter (nm) for the size bin i

n_i = Particle number concentration in the size bin i

Mass distribution can also be represented *figure 5.12* in the similar way as Normalized size distribution. The mass distribution of particles in respective size bins are calculated using IPSD method. EEPS measures particles from 5.6nm-560nm whereas ELPI classifies particles 6nm-10,000nm. As EEPS cannot measure particles beyond 560nm and hence there is a discontinuity in the EEPS graph after the size range. The fine and Ultra fine particulate matter do not contribute to most of the particulate mass but are higher in number. Whereas the coarser particles are lesser in number but contribute majority to the total mass of particulate matter.

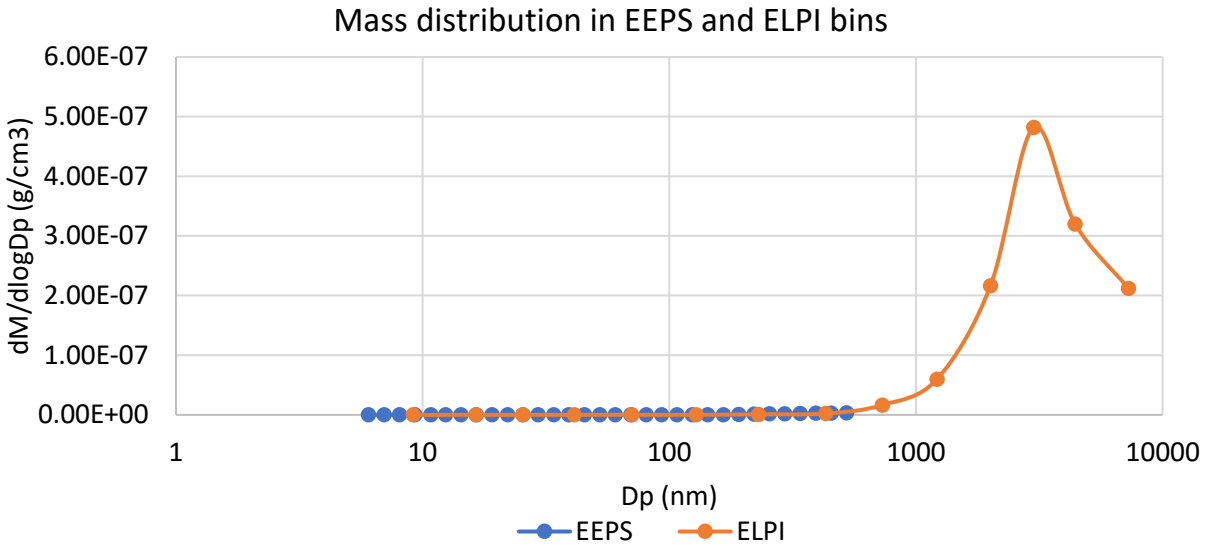


Figure 5.12 Comparison of Mass distribution in EEPS and ELPI

5.6.2 ELPI Gravimetric method (offline mass)

The impactor stages in ELPI can be used to measure the mass of the particles which are classified according to the cut off sizes. The collection substrates are placed on all the impactor stages with a size diameter of 25 mm each. The particles deposited on the substrate are used for the gravimetric and chemical analysis. The substrate material should be thin, smooth without any holes or pores to prevent any losses in collection efficiencies and cut points. Generally, aluminium foil is widely used in gravimetric measurements. It is cheap and easy to handle but only limited type of chemical analysis can only be performed with it [28].

Particle bounce occurs when the particles being sampled are dry and solid. This reduces the collection efficiency of the particles. So to avoid or minimize this, the collection substrate is coated with grease to improve collection efficiencies and to get more accurate results [28].

6 Results

The following chapter discusses the particulate emissions from the brake pads tested on the sections of test procedures ISO 26867 and SAE J2522 and newly developed WLTC. The test data of Zimmerman and Ferodo brake pads from ELPI instrument could not be compared with EEPS data due to some data logging issues during the experiment. Considering this situation, data from EEPS was only presented for Zimmerman and Ferodo pads wherever applicable. Since the sequence of test procedures ISO 26867 and SAE J2522 were temperature controlled, the total number of particles emitted in each brake event can be calculated by the integration of the product of particle number concentration times the tunnel flow (Tunnel flow is 2400 m³/h).

6.1 Particle emissions of brake pads

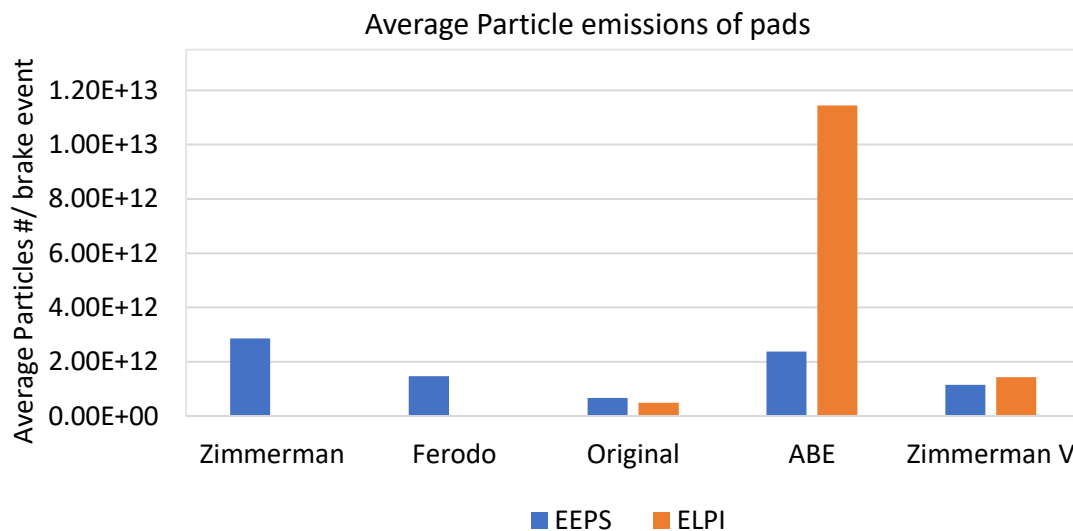


Figure 6.1 Average particles emitted from brake pads

Figure 6.1 summarizes the average particles emitted from the brake pads tested. Particles produced in the test sections of A and B were not considered due to the fact that the brake pads were new and the production of particles were relatively higher due to the wear of the resin on the pad contact surface and non-uniformity at the contact surface

of friction pair. The ordinate value was obtained by averaging the particles produced from the sections (C to K) for the respective pads. Among the four pads, Zimmerman, Zimmerman V, Ferodo and ABE average particle number produced were in orders of 10^{12} while Original pad produced in the orders of 10^{11} and was the lowest among the pads tested here. ELPI value of Original and Zimmerman V were in good agreement with EEPS values showing that Original brake pad has the lowest average particle emissions.

6.2 Particle emissions from F, G, H and K section (EEPS)

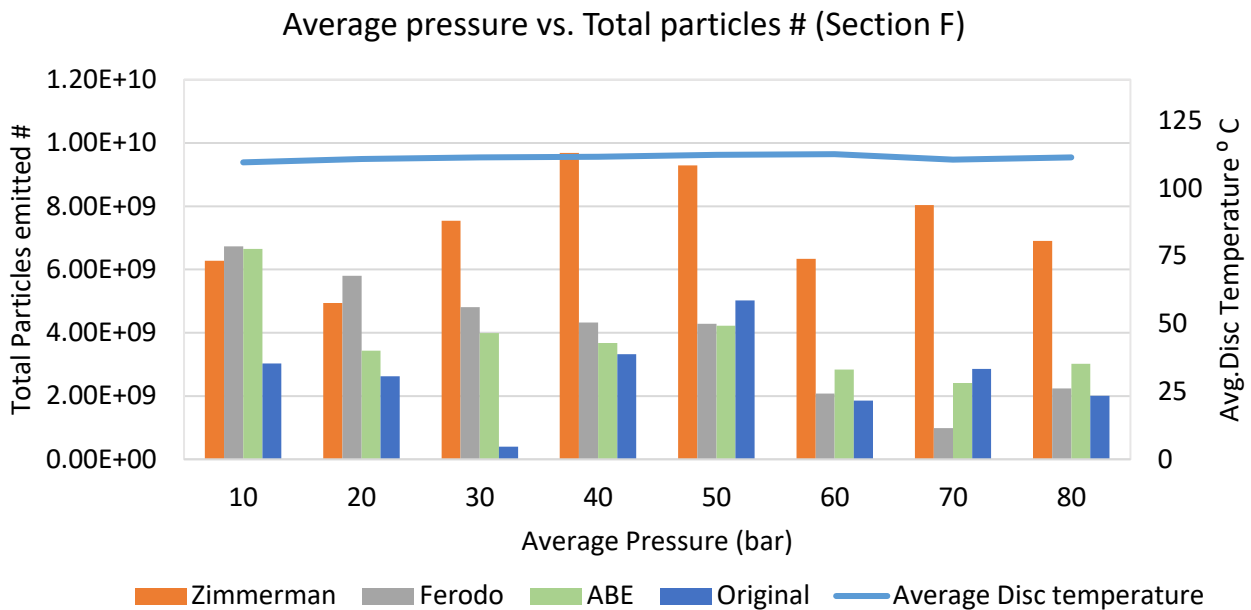


Figure 6.2 Particle emissions on test section F

The particle emissions from the pads depends on the conditions of braking and the composition of the brake pad material. *Figure 6.2* shows the total particles emitted from brake pads in the test section F. The disc has initial brake speed of 40kph and release speed of 5kph which translate to a kinetic energy of 46kJ. The average pressure on the brake disc was increased in steps of 10 bar consecutively after each brake application. The initial and final disc temperatures are 100 °C and 120 °C with average disc temperature around 110 °C. Total particles emitted were in the order of 10^9 for all the brake pads and irrespective of the applied pressure as shown in *figure 6.2*. Particle

emissions from Zimmerman increased until 40 bar and then started to decrease thereafter but still higher compared to the other pads. Overall, average emissions from Zimmerman were highest among the rest of the pads. Particles emitted from Ferodo decreased gradually as the average pressure was increased and has the lowest average particle emissions over this section as shown in *figure 6.3*. ABE and Original do not show any increase in particles with increase in average pressure like Zimmerman. There are no noticeable ultrafine particles in this section of braking regime in all the brake pads. *Figure 6.3* shows the particle size distribution in the EEPS averaged over the entire section F for the respective brake pads. From this *figure 6.3* particles from Zimmerman contributed majority to the mass of the particles emitted followed by ABE, Original and Ferodo. Fine and coarse particulate matter contribute majority to the total particulate mass rather than ultrafine particulate matter.

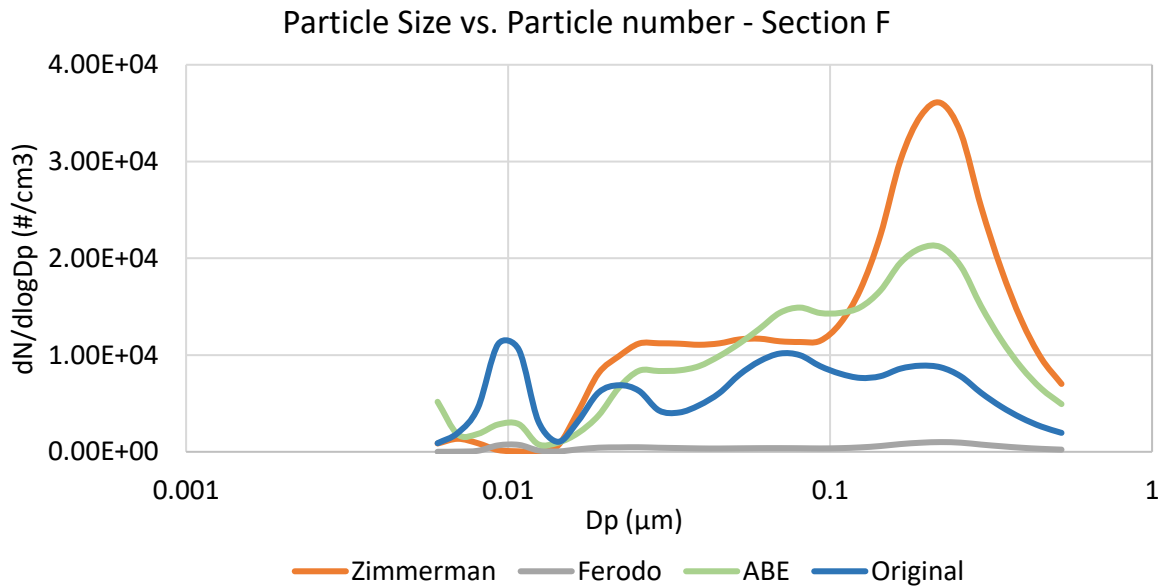


Figure 6.3 Average Particle Size Distribution - Section F

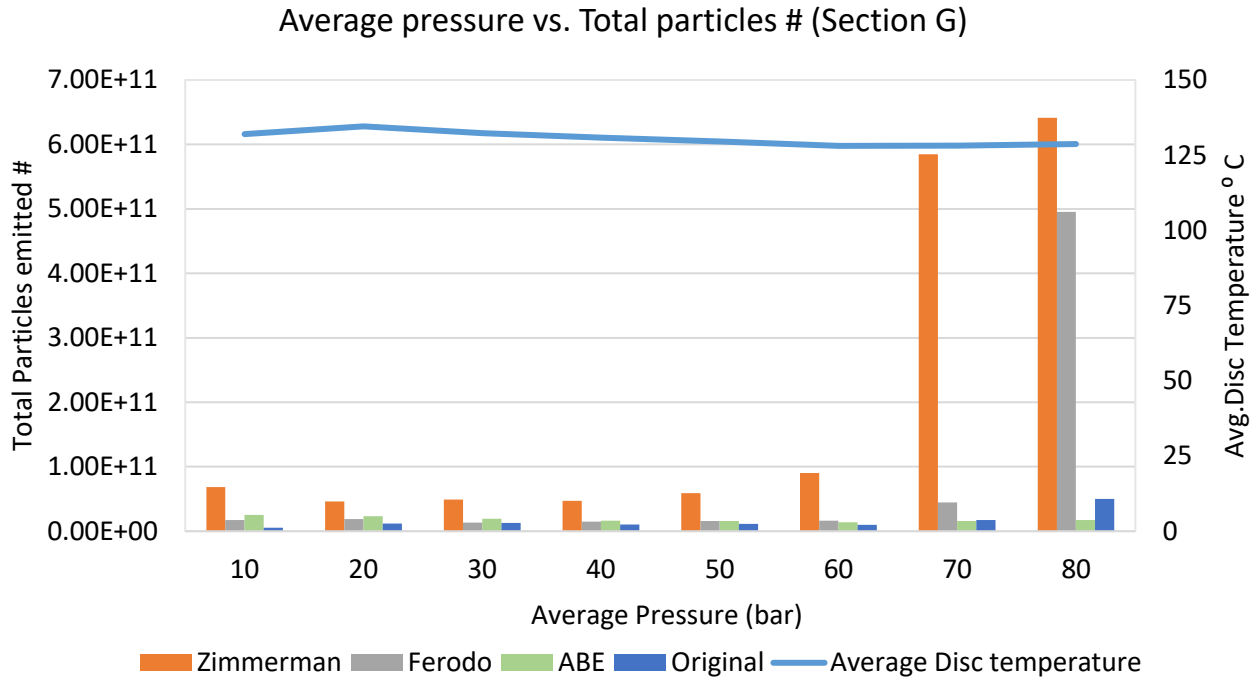


Figure 6.4 Particle emissions on test section G

The section G of the test procedure *figure 6.4*, the initial and final temperature of the disc was 100 °C and 160 °C with average temperature of around 130 °C respectively. The brake speed was 80 kph and release speed was 40 kph which translates to a kinetic energy of 140kJ. With the increase in average pressure in steps of 10 bar, all the four pads produced particles in order of #10¹⁰ until the average pressure of 60 bar. The increase in particle emission order to #10¹⁰ was due to the increase in average disc temperature when compared to previous section F. The subsequent increase in average pressure to 70 bar had shown that particles emitted from Zimmerman had increased significantly to order of #10¹¹ while other pads still in the orders of #10¹⁰. The next increase in average pressure to 80 bar made Ferodo to emit particles in the orders of #10¹¹ which was almost equal in particle number with Zimmerman. The remaining pads ABE and Original were consistently in the orders of #10¹⁰ exhibiting no influence on the increase in average pressure.

Figure 6.5 shows the particle size distribution averaged over the section G. The increase in particle emissions from Zimmerman and Ferodo contributed to increase particles in Ultra fine region (PM_{0.1}) and in fine region (PM_{2.5}) for Zimmerman and followed by Ferodo. ABE and original had almost the same number of particles throughout all the size bins.

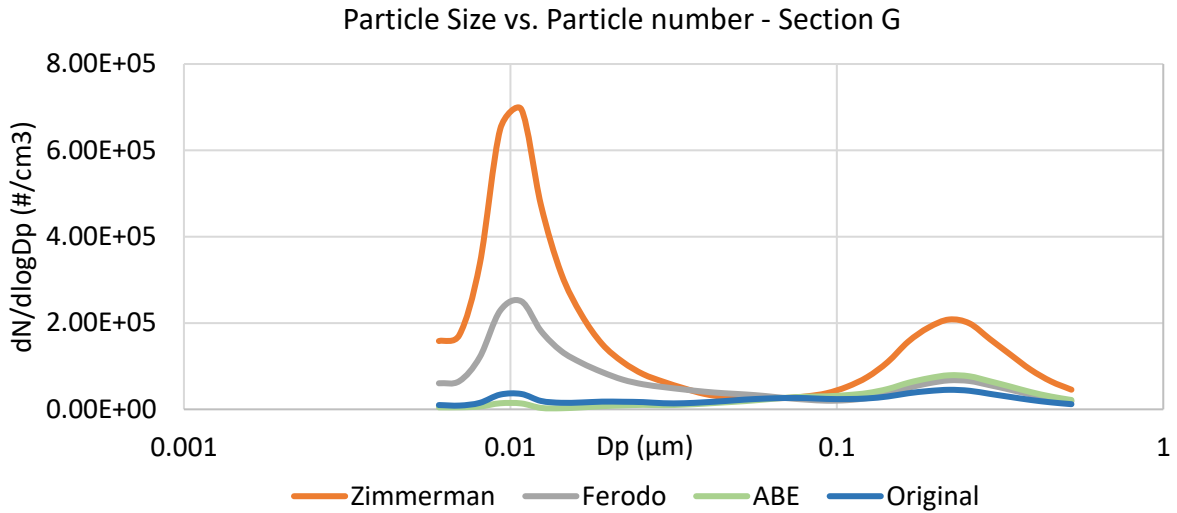


Figure 6.5 Average Particle Size Distribution - Section G

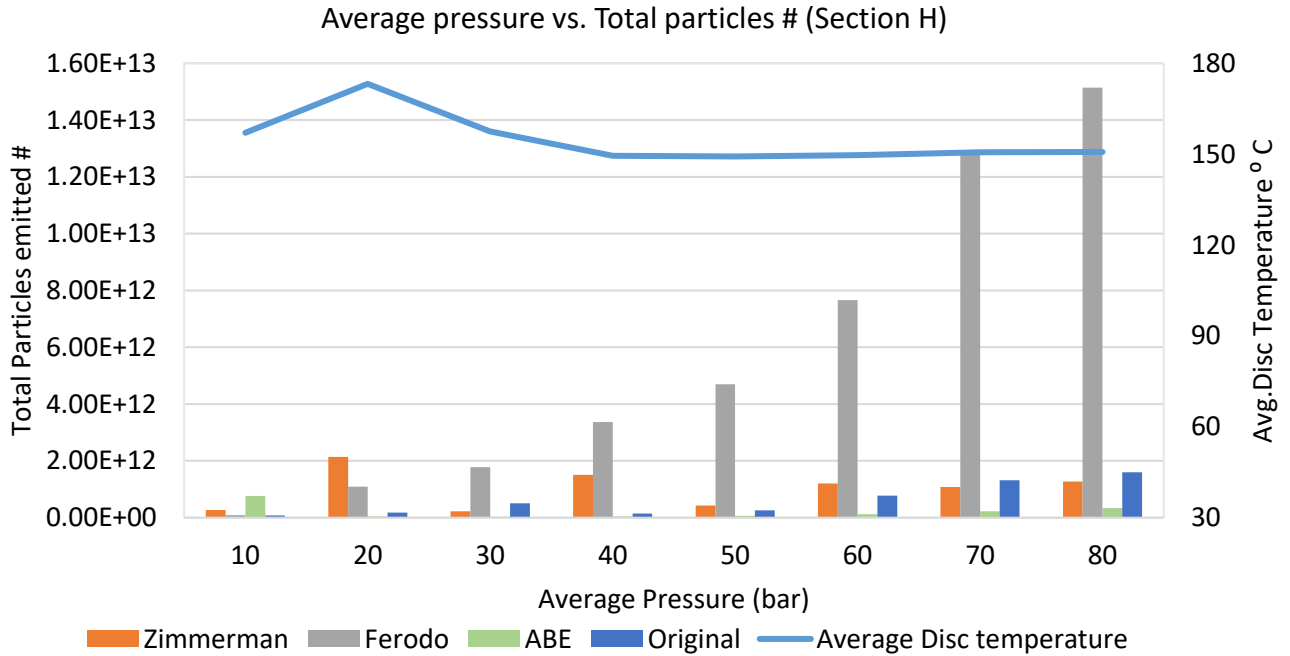


Figure 6.6 Particle emissions on test section H

The Section H *figure 6.6* of the test procedure was of relatively high energy dissipation compared to the previous sections G and F. Initial and final disc temperatures were 100 °C and 210 °C with average disc temperature of 150 °C. Brake speed was 120 kph and release speed was 80 kph which translates to a kinetic energy of 230 kJ to be dissipated through friction surface. The consecutive increase in the average brake pressure in steps of 10 bar had significant increase in generation of particles emitted from Ferodo. It increased from the orders of $\#10^{10}$ at 10 bar to $\#10^{13}$ at 80 bar. Brake pad Original emitted higher particles as the pressure increased but did not show any step change in particle numbers as in the case of Ferodo. The total particles produced were in the orders of $\#10^{10}$ at 10 bar and then increased gradually to $\#10^{12}$ at 80 bar. ABE also emitted higher particle numbers as the average pressure continued to rise but confined to particle numbers in the order of $\#10^{11}$. Particles from Zimmerman were consistently at the same level in the orders of $\#10^{12}$ showing no strong dependence of particles emitted with respect to increase in average pressure.

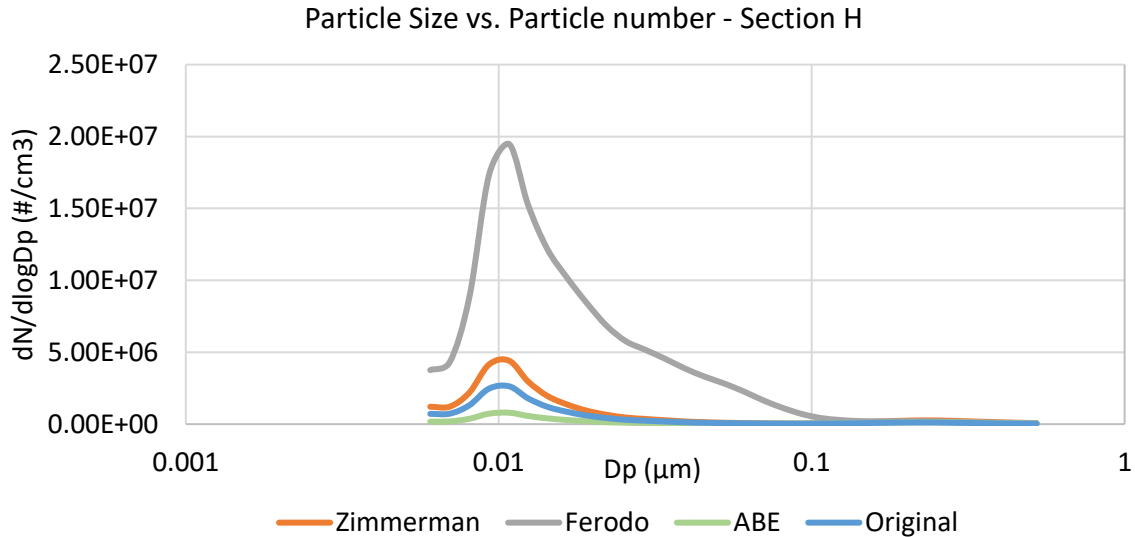


Figure 6.7 Average Particle Size Distribution - Section H

Figure 6.7 shows the average particle size distribution on the test section H. The higher particles from Ferodo resulted in increase in particle numbers in ultra fine region (PM_{0.1}). The average particles produced were in the orders of $\#10^7$ for Ferodo followed

by Zimmerman and Original in the orders of $\#10^6$ in the same region. ABE had the lowest average particles produced in this section which is in the order of $\#10^5$.

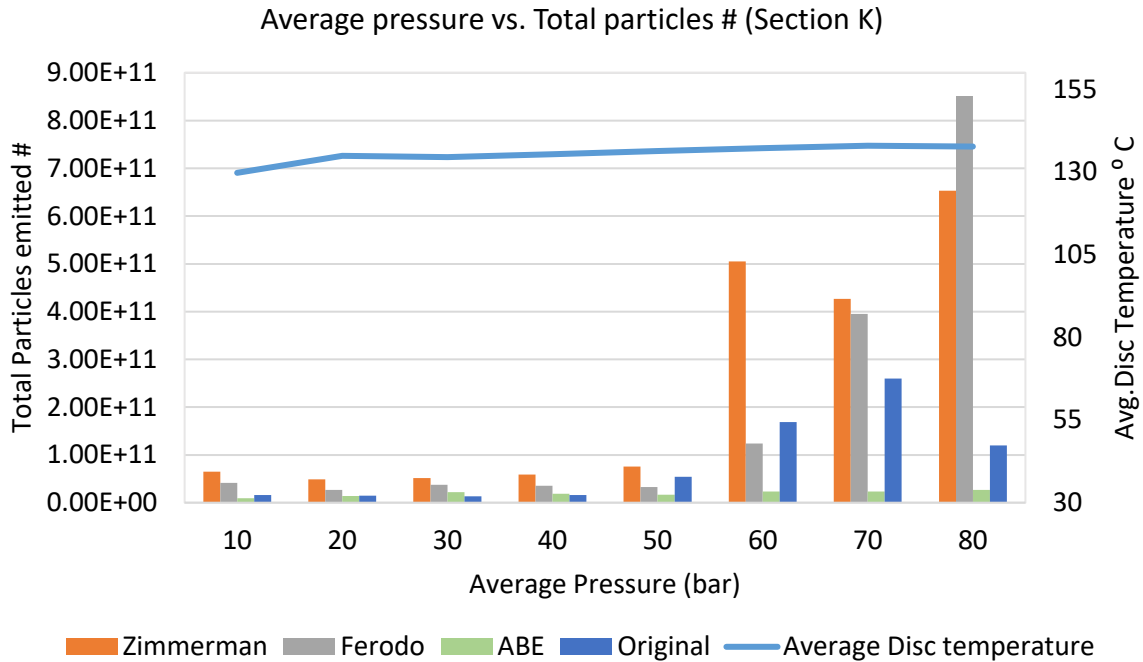


Figure 6.8 Particle emissions on test section K

Figure 6.8 shows the total particles emitted from brake pads over the section K. Initial temperature of the disc was 100 °C and final temperature was around 170 °C with average temperature of 135 °C. The average pressure is increased in steps of 10 bar starting with 10 bar initially and incrementing successively up to 80 bar. Brake speed was 80 kph and release speed was 30 kph which translate to a kinetic energy of 160 kJ. In this section of braking regime, Zimmerman, Ferodo and Original emitted higher particles after 50 bar increasing from orders of $\#10^{10}$ to $\#10^{11}$ with Zimmerman and Ferodo showing significant rise in particle numbers. Particles from ABE were almost the same throughout in orders of $\#10^{10}$ indicating that this pad had no good relationship with rise in average pressure in this section of test procedure. Figure 6.9 shows the particle size distribution in size bins of EEPs averaged over the braking events in this section. Zimmerman produced the highest average number of particles in both fine and ultrafine region followed by Ferodo, Original and ABE.

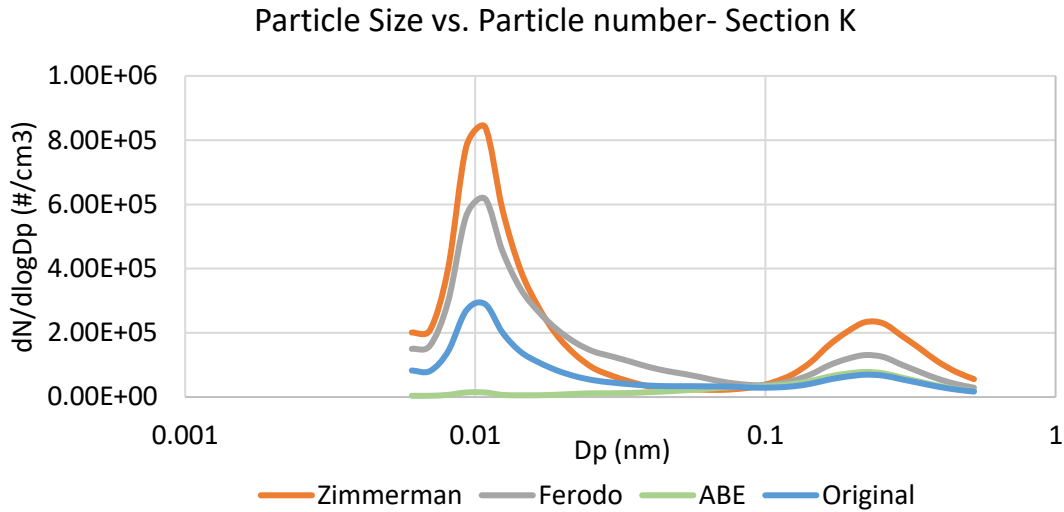


Figure 6.9 Average Particle Size Distribution - Section K

6.3 Dissipated Power on Particle emissions

The following graphs show the total particles emitted for each brake event based on the dissipated power and work. The initial temperature of the disc was 100 °C and final temperature of the disc ranges between 120 °C and 220 °C. The particles emitted from the brake pads were strongly dependent on the energy and average power dissipated as in the case of Original, ABE and Ferodo but quite different in case of Zimmerman.

Polynomial function of 2nd degree was used to show the correlation between the variables which is in the form of ax^2+bx+c where a, b, c are constants and x is the average power dissipated. Although there was no literature evidence for the use of polynomial equation, it was used to show the strength of the relation between the average power and particle emissions. *Figure 6.10* compares the total particles emitted from each braking event and its dependence on average power dissipated of both ELPI and EEPs instruments of Original brake pad. The particles produced were in the orders of #10⁹ until the average power of 50 kW and thereafter increased to higher number orders.

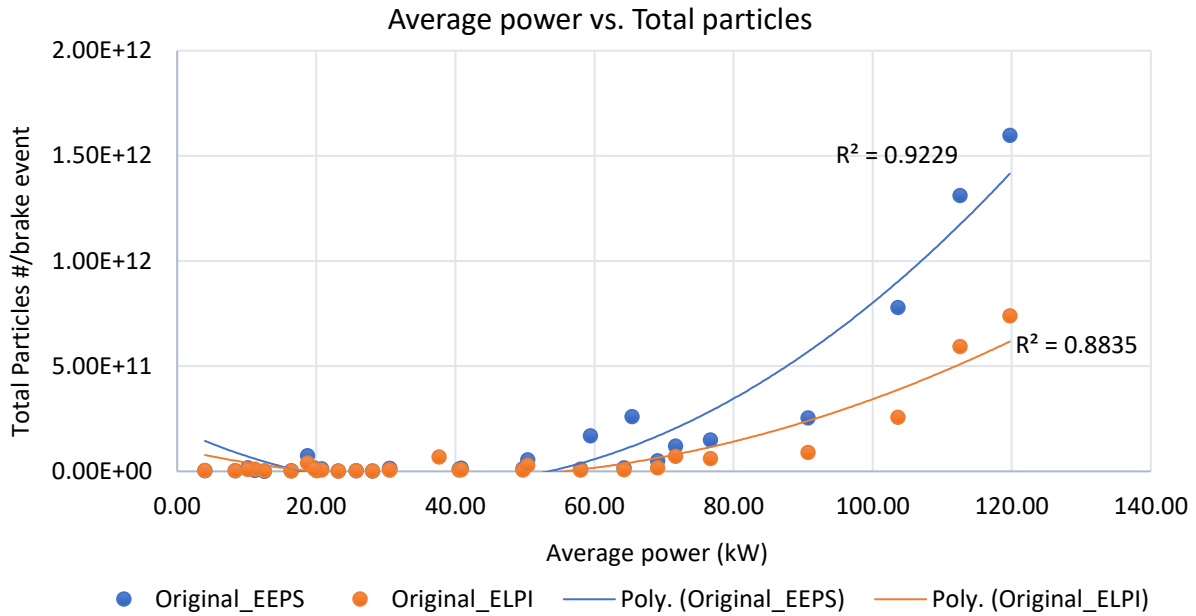


Figure 6.10 Dependence of total particles emitted on average power (Original)

Figure 6.11 shows the total particles emitted from ABE brake pad with increase in average power dissipated. The particle numbers are in the order of $\#10^{10}$ until around 70 kW and increase to higher order subsequently. Both EEPS and ELPI have good agreement in terms of the particle numbers.

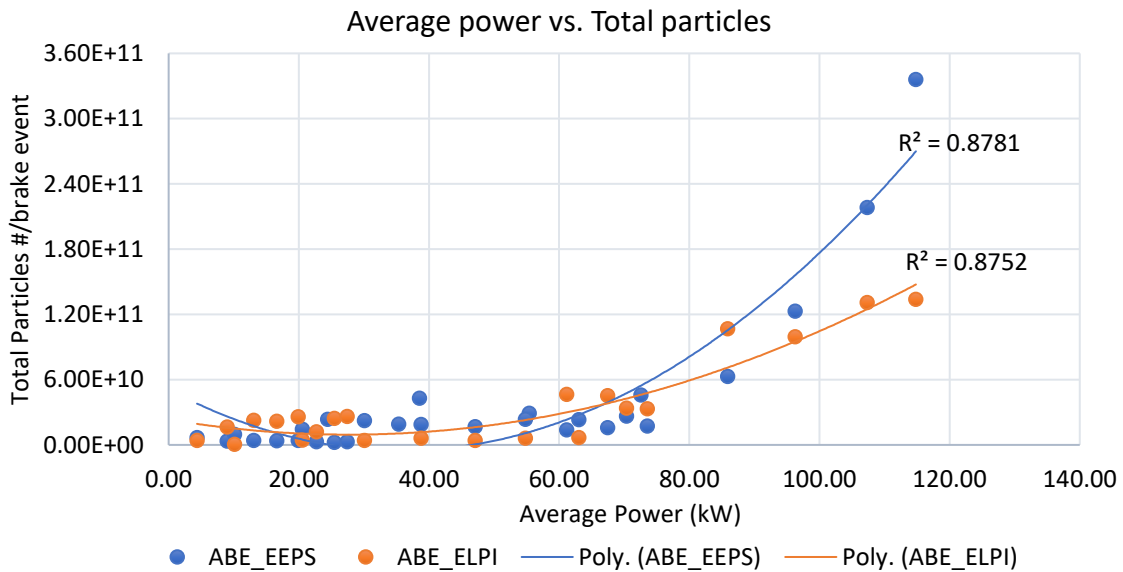


Figure 6.11 Dependence of total particles emitted on average power (ABE)

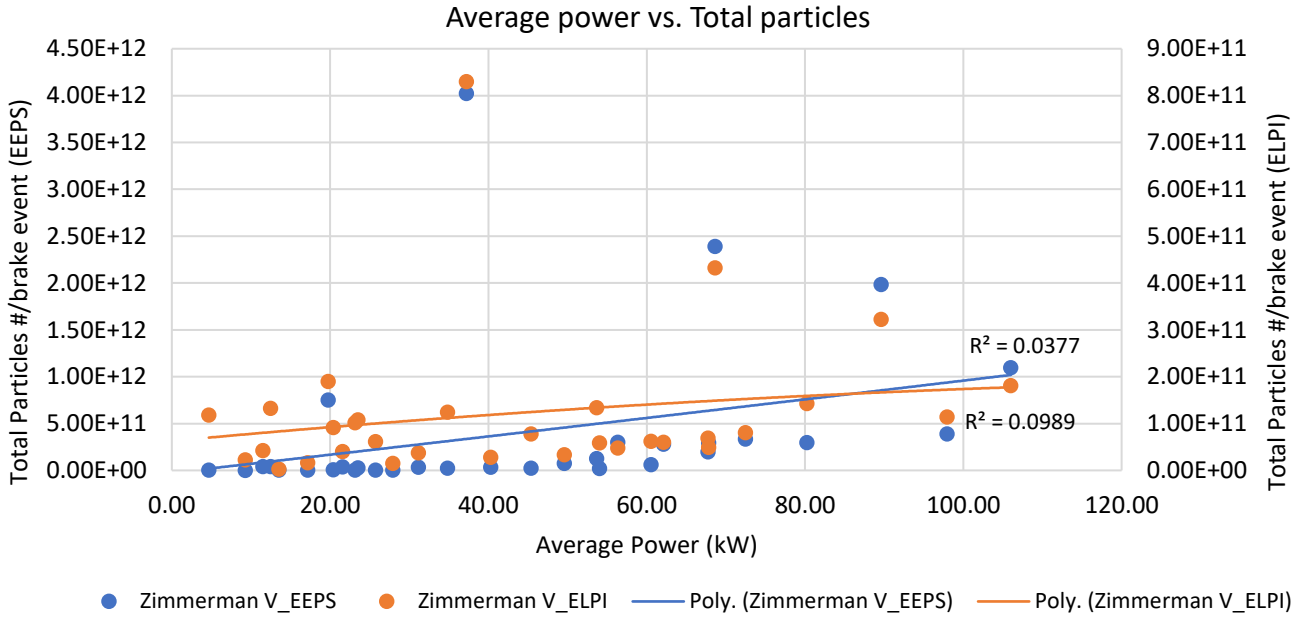


Figure 6.12 Dependence of total particles emitted on average power (Zimmerman V)

As the ELPI data of Zimmerman is not available, Zimmerman V is considered for the comparison as the data set used here matches with Zimmerman. This pad is quite different when compared to Original and ABE pad. The particle emissions are relatively higher at lower average power with the trend showing no strong correlation with average power. Both the instruments show similar trend with the increase in average power indicating that particle emissions from this pad are not dependent upon average power dissipation as shown in *figure 6.12*.

The particles emitted from Ferodo brake pad increase with increase in average power dissipation as shown in *figure 6.13*. The emission rate starts from as low as in the order of $\#10^9$ at lower average power and increases all the way to $\#10^{13}$ at the highest average power. The correlation was strong suggesting that particle emissions increase as the power dissipation increases. Ferodo also produced highest particle emissions compared to other pads at highest average power dissipation. *Figure 6.14* shows the particles emissions at the highest average dissipated power for all the four pads. Ferodo emitted particles in the orders of $\#10^7$ whereas the emission rates from remaining pads were in the orders of $\#10^6$ with ABE having the lowest particle number.

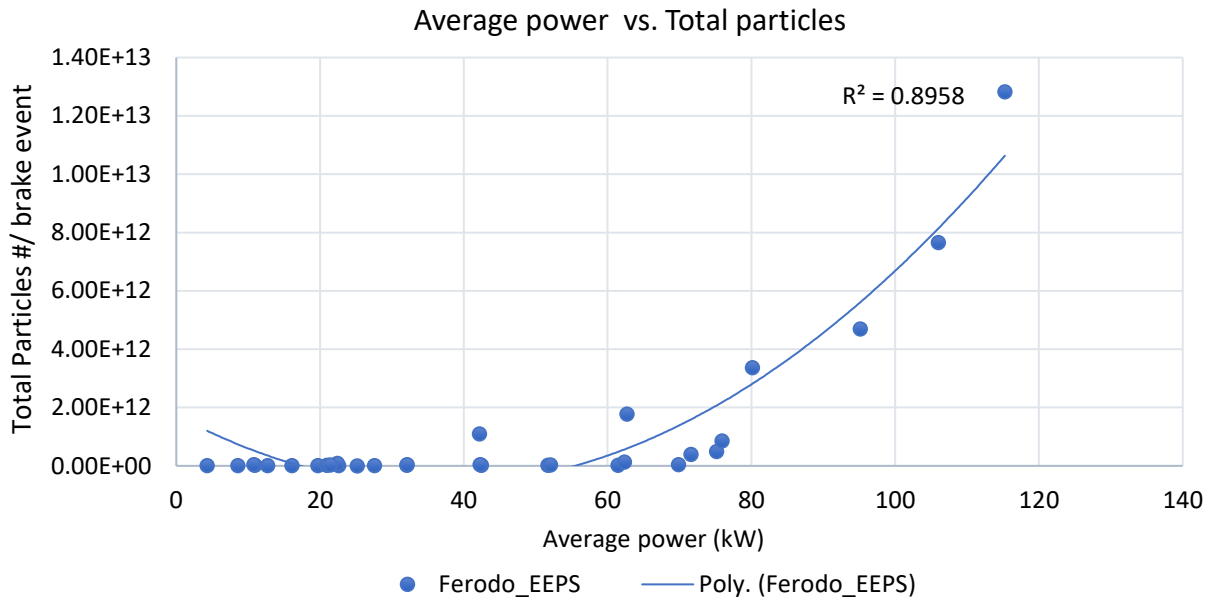


Figure 6.13 Dependence of total particles emitted on average power (Ferodo)

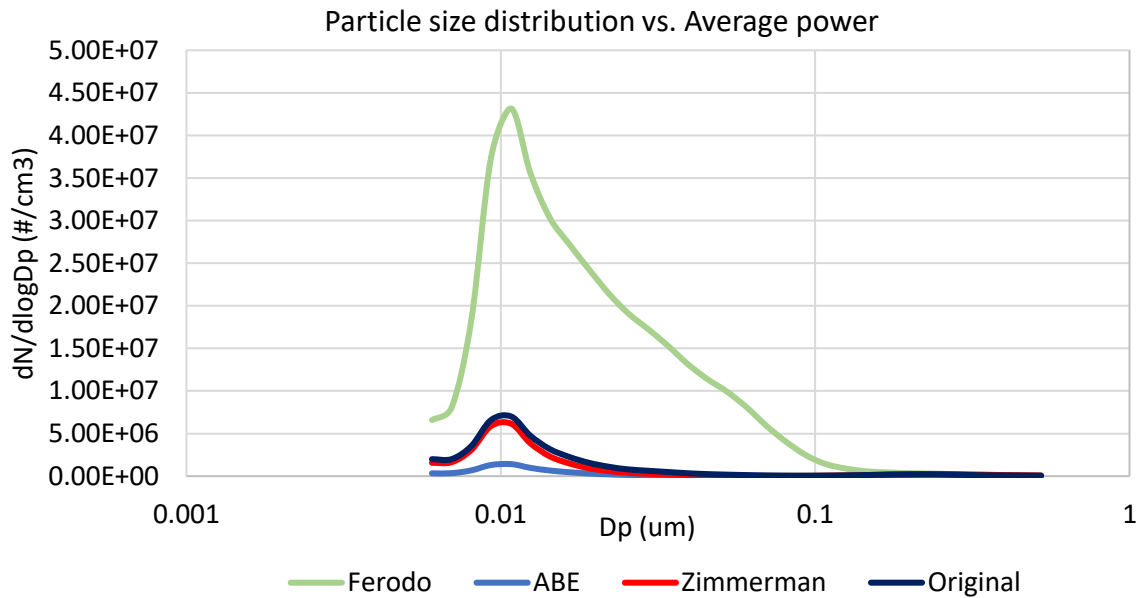


Figure 6.14 Particles emissions at highest average power dissipation

6.4 Particle emissions for unit energy dissipation

The particles emitted from the brake pads Zimmerman, Ferodo, Original and ABE can be expressed in terms of particles/kJ to know the particles produced for unit energy dissipated. The total particles produced on the sections C to K are added and divided by the total energy dissipated in these sections. Zimmerman had the highest number of particles produced per unit energy dissipation as shown in *figure 6.15*. ABE and Zimmerman were almost at the same magnitude in the orders of 10^{10} and Original had the lowest particles/kJ. The data from EEPS was used for this comparison in *figure 6.15*.

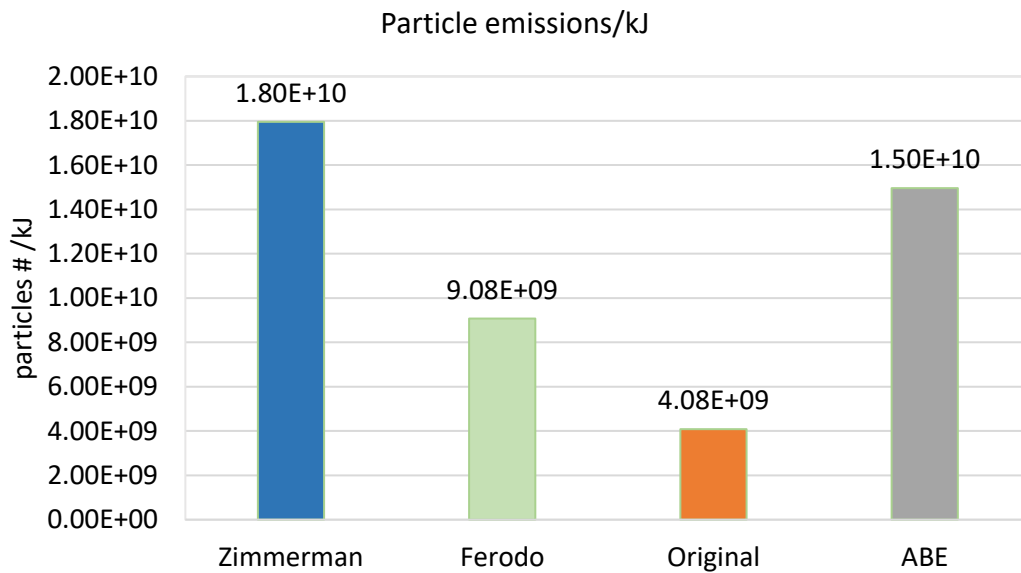


Figure 6.15 Comparison of particle emissions with respect to unit energy dissipation

The data of EEPS and ELPI from sections F, G, H and K of SAE/ISO were compared with regards to the particles emitted per unit energy dissipation and average power. The particles emitted from each braking event of the corresponding section is divided by the energy of that section to get particles/kJ. *Figure 6.16* shows the particles produced from kJ of energy dissipated with increase in average power from Original brake pad. Particles produced in each braking event was divided by the total energy dissipated in that braking event to get particles produced per kJ. The data from both the instruments were in good agreement suggesting that particle emissions/kJ increase with increase in average power

dissipation. The increase was from the orders of # 10^7 particles/kJ at lower average power and increases significantly up to the order of # 10^9 particles/kJ.

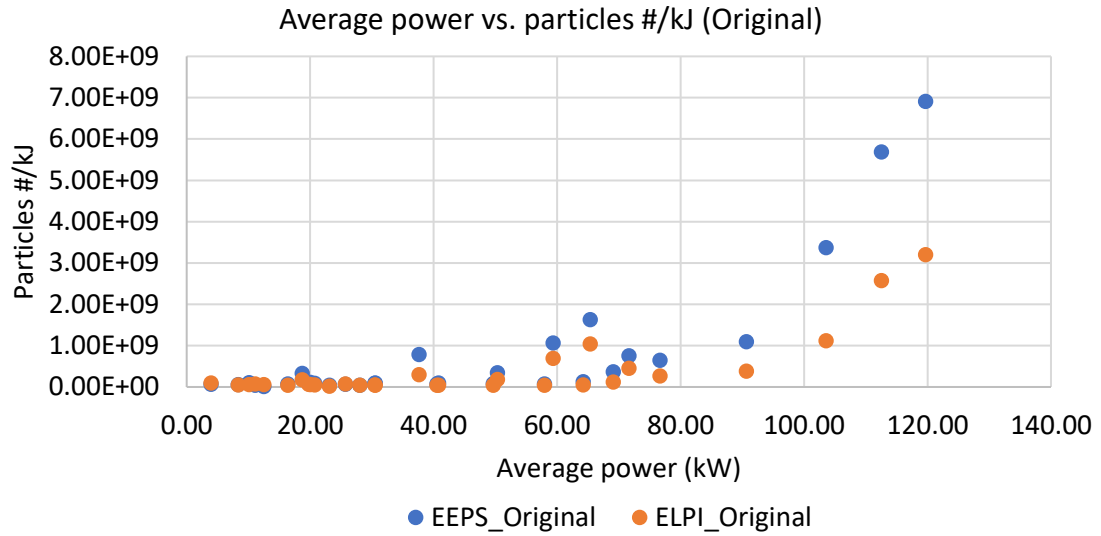


Figure 6.16 Particles/kJ emitted with respect to average power dissipation (Original)

Figure 6.17 shows the particles produced per kJ of energy dissipation with increase in average power from ABE brake pad. The increase in particles were seen after the average power of around 70 kW. EEPS and ELPI show the similar trend of increase in particle emissions.

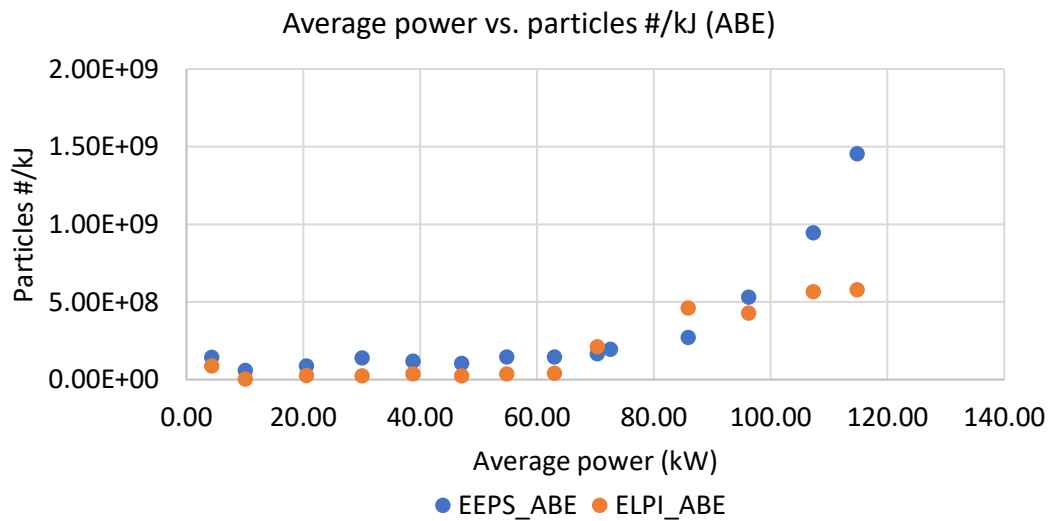


Figure 6.17 Particles/kJ emitted with respect to average power dissipation (ABE)

particles/kJ emitted among other pads. It is seen clearly that at peak average power, the particles emitted per kJ were in the orders of $\# 10^{10}$.

6.5 Particle emissions dependence on Disc Temperatures.

The particle emissions were evaluated against change in initial and final disc temperatures when all the braking parameters were kept constant. Parameters such as average pressure, energy and power dissipated were held constant to evaluate the change in particle emissions with change in initial and final disc temperatures.

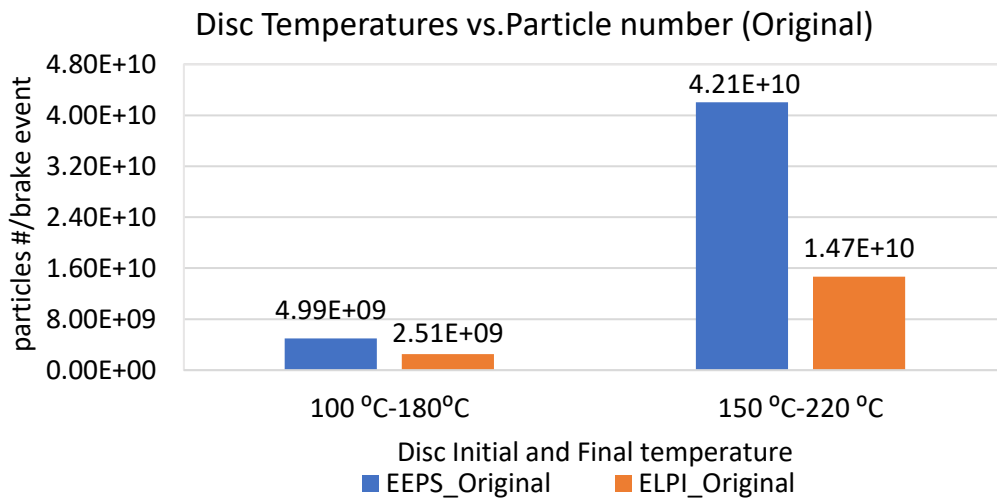


Figure 6.20 Particle emissions with regards to temperature of disc (Original)

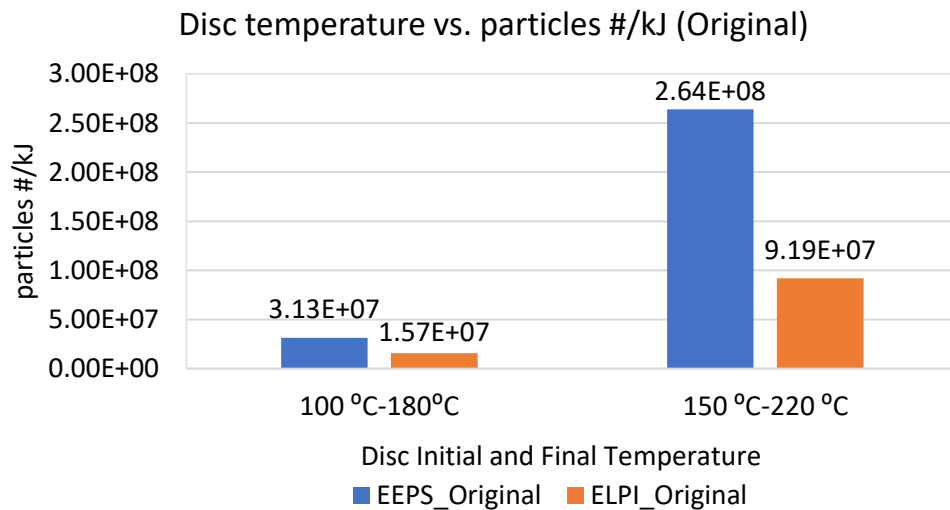


Figure 6.21 Particle emissions per kJ of energy dissipated (Original)

Figure 6.20 shows the particle emission per brake event with regards to initial and final temperatures of disc from Original brake pad. Initial and final temperatures of the brake disc were increased from 100 °C to 180 °C and from 150 °C to 220 °C respectively. The average pressure in the line was 30 bar with 159 kJ of energy to be dissipated at constant average power of 30 kW. The particles emitted increased from #10⁹ to an order of #10¹⁰ for this pad showing that increase in temperature increased the particles emissions. Figure 6.21 shows the particles emitted per kJ energy dissipated. The particles produced in the brake event was divided by the kinetic energy dissipated. Figure 6.22 and figure 6.23 shows the particle size and mass distribution. It is clear that increase in temperature of the disc had influence on the fine particulate matter and increase in the fine particles leads to increase in particulate mass concentration which amounts for considerable total particulate mass. The particles in Ultra fine region (UFPs) remained more or less the same even with increase in disc temperature.

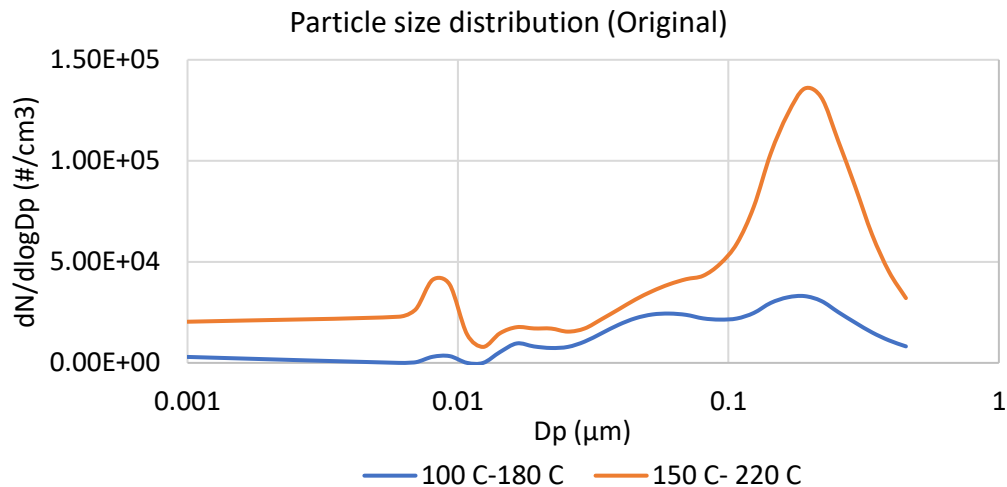


Figure 6.22 Variation of particle size distribution with respect to temperature (Original)

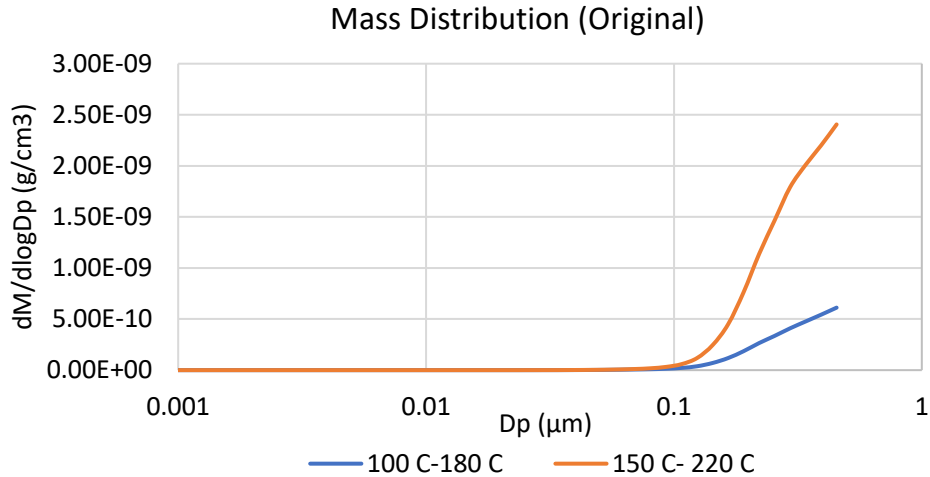


Figure 6.23 Variation of Mass distribution with respect to temperature (Original)

Figure 6.24 shows the dependence of particle emission from a single brake event with regards to different initial and final disc temperatures of ABE pad. The similar trend was shown by ABE pad like the Original pad. Figure 6.25 shows the particles per kJ of energy dissipated for the respective brake event. The particles emitted increased with increase in initial and final disc temperature and this increase was dominated by the fine particulate matter as shown in size distribution figure 6.26. Increase in fine particulate matter leads to increase in particulate mass emission as shown in figure 6.27.

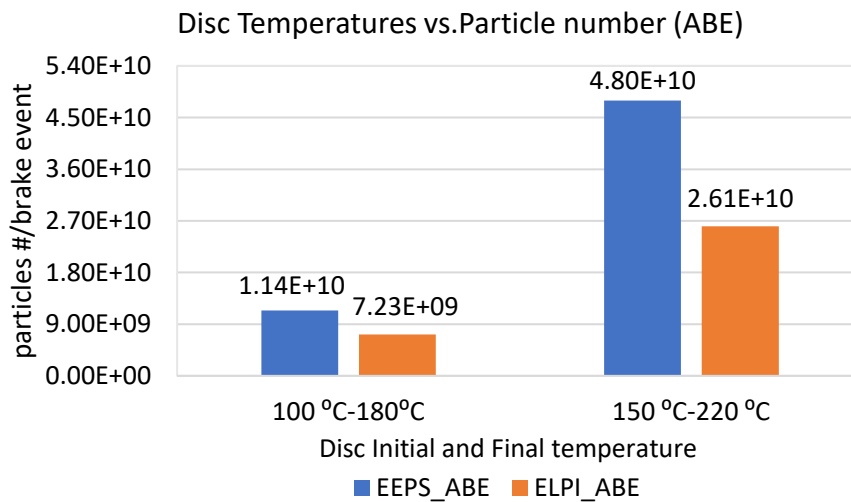


Figure 6.24 Particle emissions with regards to temperature of disc (ABE)

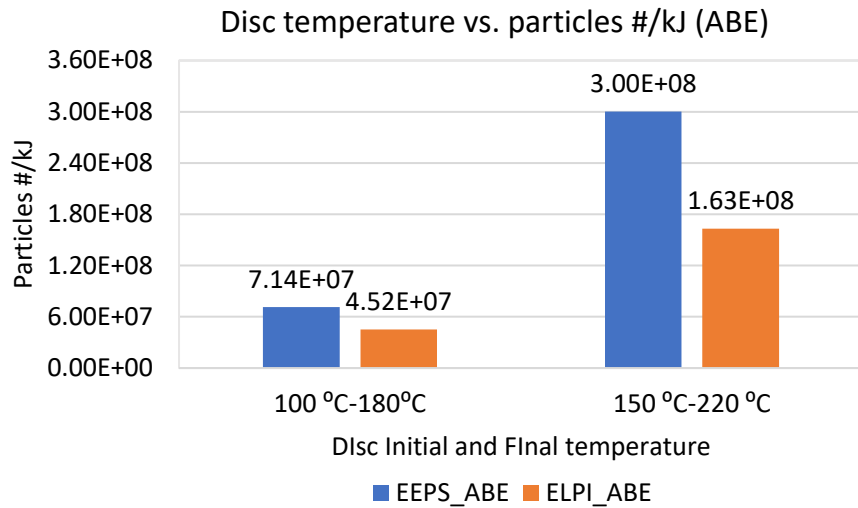


Figure 6.25 Particle emissions per kJ of energy dissipated (ABE)

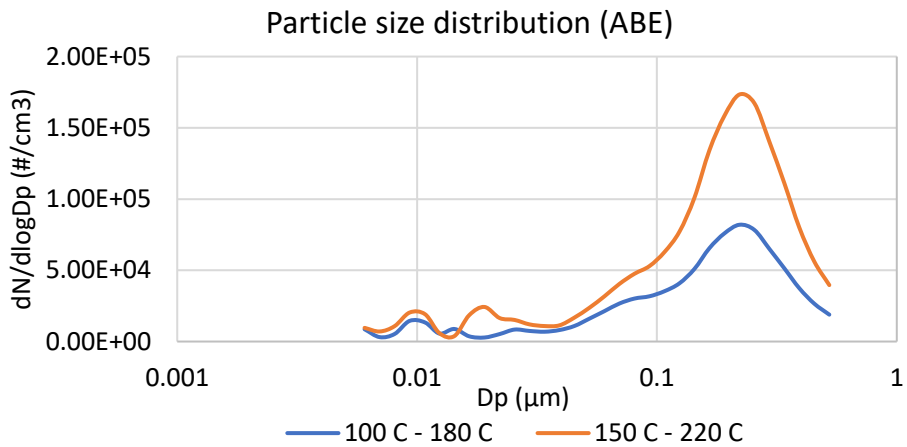


Figure 6.26 Variation of particle size distribution with respect to temperature (ABE)

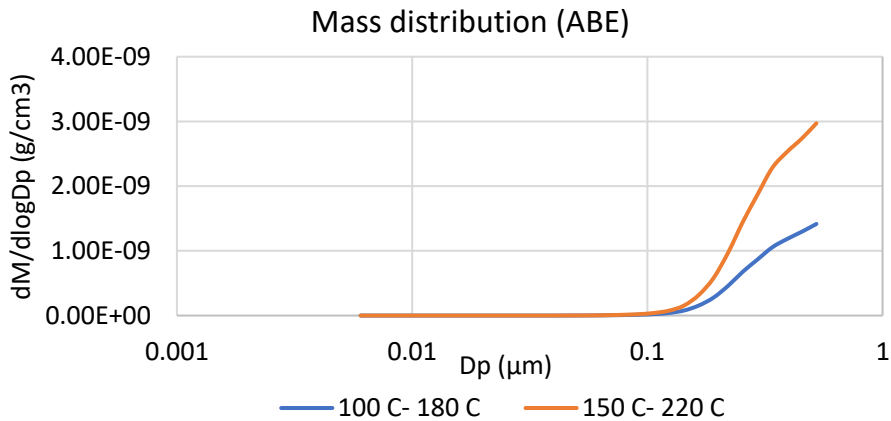


Figure 6.27 Variation of Mass distribution with respect to temperature (ABE)

Figure 6.28 shows the particles emitted from Zimmerman pad for a single brake event when the initial and final temperature of disc were increased. Figure 6.29 shows the particles produced per kJ of energy dissipated for the respective brake event. As seen with Original and ABE, there was an increase in particle numbers emitted with the increase in particles concentrated in fine particulate region. Figure 6.30 and figure 6.31 shows the particle size and mass distributions for the above conditions.

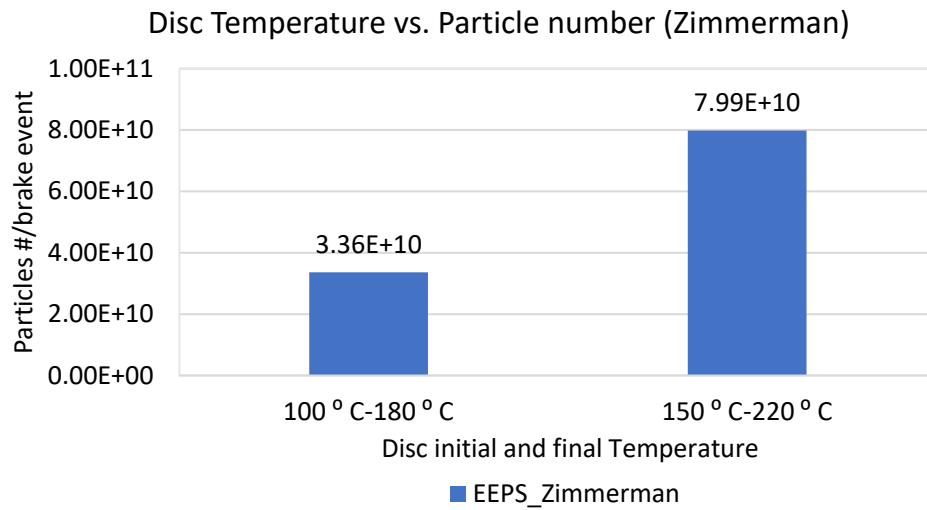


Figure 6.28 Particle emissions with regards to temperature of disc (Zimmerman)

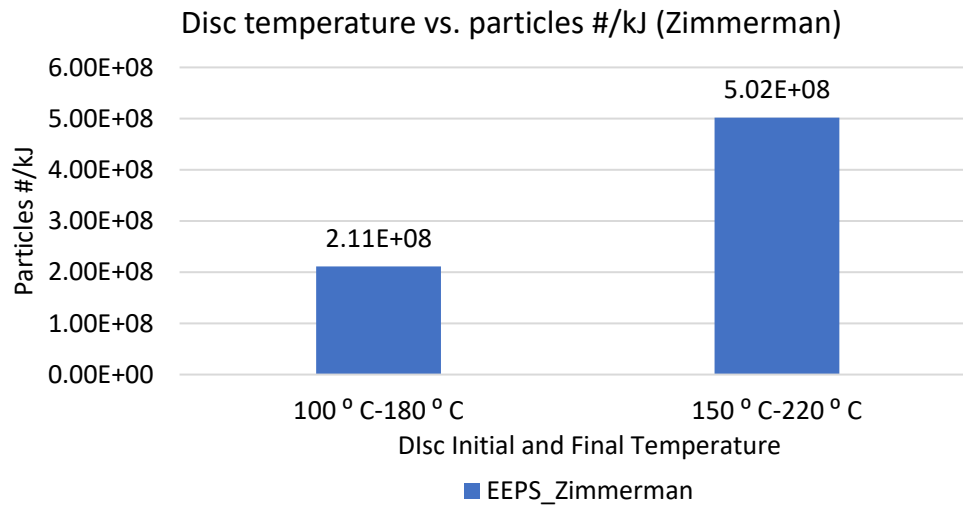


Figure 6.29 Particle emissions per kJ of energy dissipated (Zimmerman)

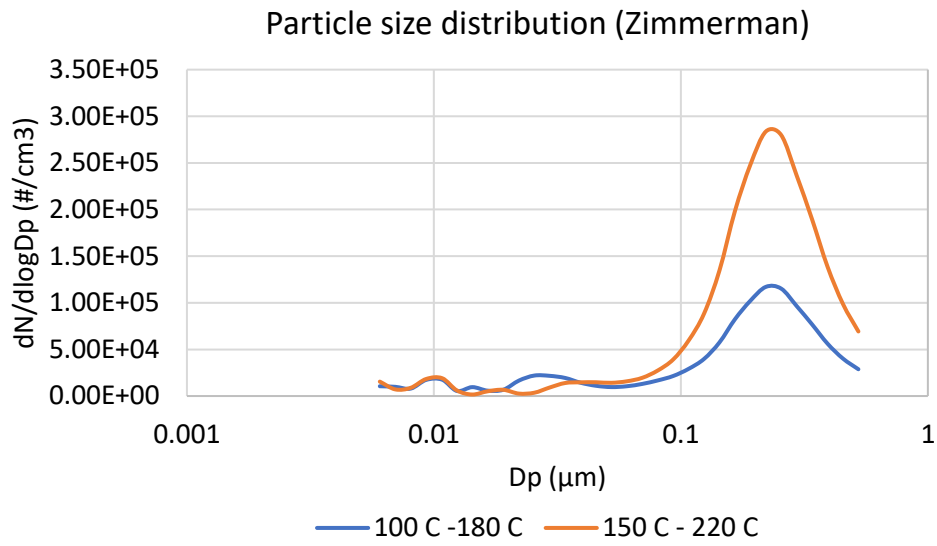


Figure 6.30 Variation of particle size distribution with respect to temperature (Zimmerman)

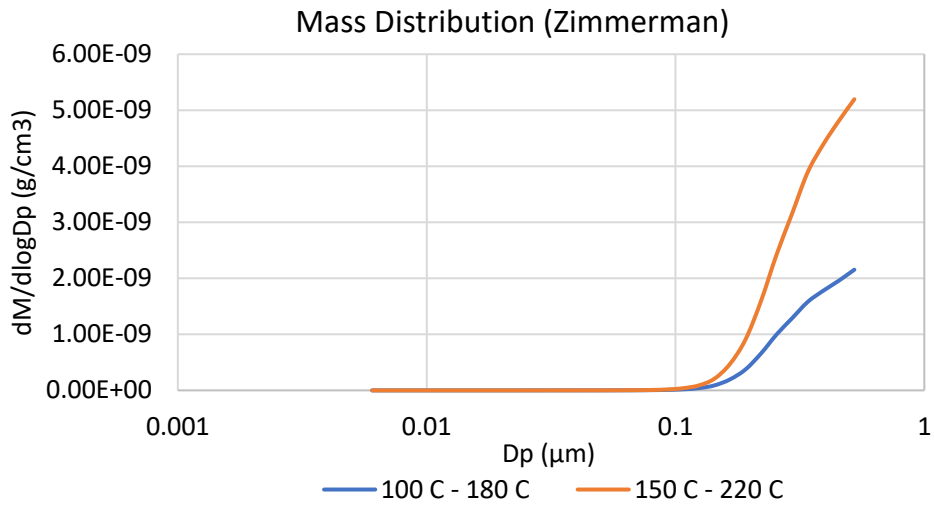


Figure 6.31 Variation of Mass distribution with respect to temperature (Zimmerman)

6.6 WLTC

The WLTC brake cycle has well defined speed profiles for all the 10 segments. Based on this, particulate emissions for each segment can be quantified in terms of emissions per km. The particle concentration from EEPS is integrated with tunnel flow rate of $2400\text{m}^3/\text{h}$ to get the total particle number (PN) in each segment. Total PN emitted divided by the distance driven in each segment gives emission in terms of Particle emission rate per km. The test was repeated for 3 consecutive times with brake pad 'Zimmerman V'. All the data presented here was from EEPS instrument.

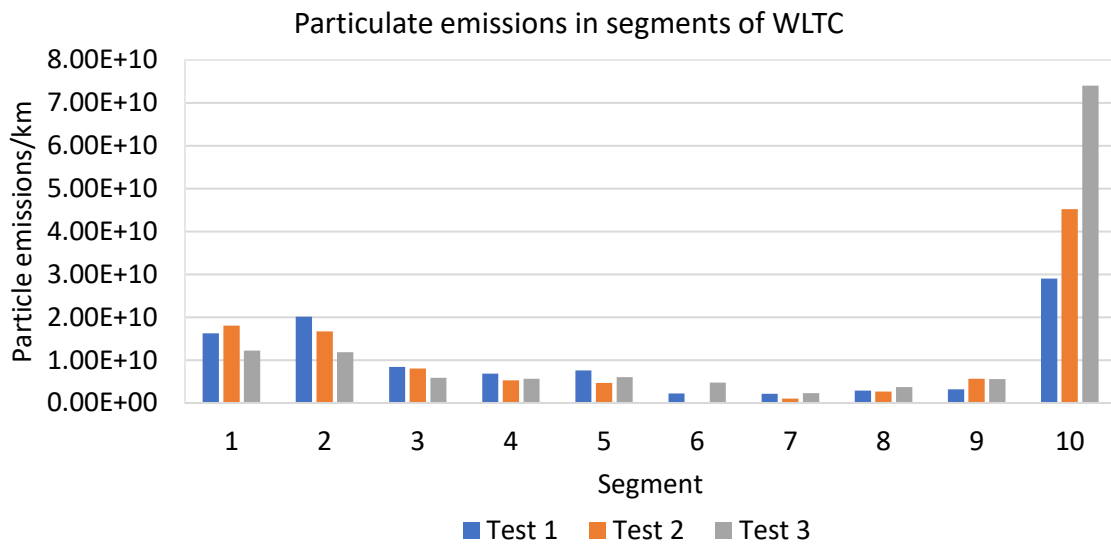


Figure 6.32 Particle emissions in each segment of WLTC

Figure 6.32 shows the particles emitted in 10 individual segments of WLTC for 3 WLTC tests without background correction. The particles emitted in each segment were in good agreement with the repetitions except the last segment i.e., the 10th segment had high particle emissions, and this influences the overall particle emissions per km. The successive tests 2 and 3 produced high particle emissions in the last segment and hence the overall particle emission per km continued to rise as shown in *figure 6.33*.

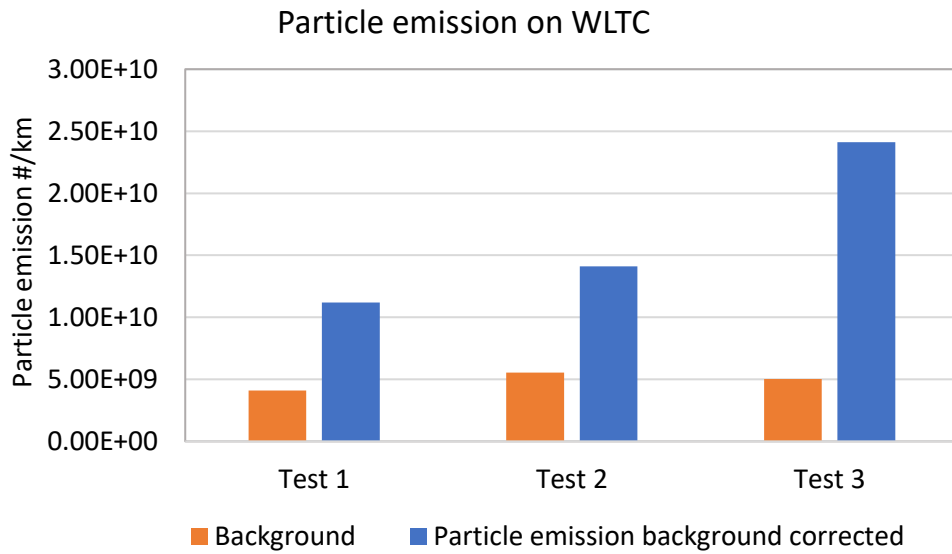


Figure 6.33 Particle emissions over 3 repeated WLTC cycles (EEPS)

Figure 6.33 shows the particle emission per km over WLTC cycle. The particle emission rate is around 1.65×10^{10} #/ km averaged over three WLTC tests after subtracting the background. The background was almost constant which is around 5×10^9 #/km. Figure 6.34 shows the particulate mass calculated for the three WLTC cycle tests. The increase in particle number emission from cycle to cycle contributed to increase in particulate mass which can be seen in the figure 6.34. Particulate mass was found to be around 0.12 mg/km which is the average value of the three WLTC repetitions.

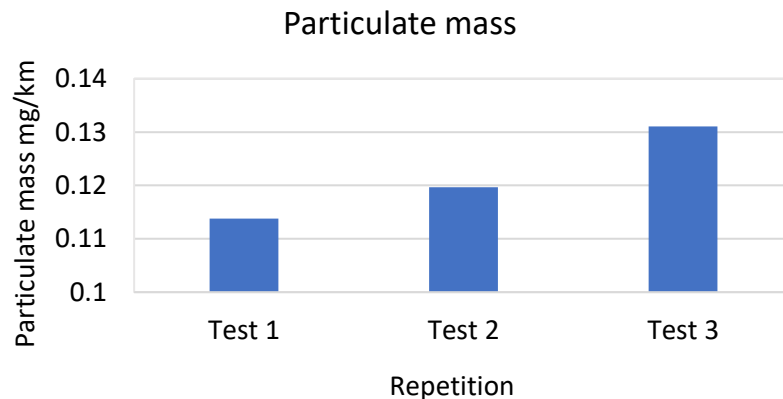


Figure 6.34 Particulate mass over the WLTC cycle calculated from EEPS

The size distribution in the *figure 6.35* corresponds to an initial brake speed of 132 kph to final brake release speed of 35 kph with initial disc temperature of 48 °C and final temperature of 217 °C. Energy and average power dissipated are 474 kJ and 31 kW. This was the most extreme braking event in entire WLTC cycle in segment 10. It is clear that high energy and power dissipation will enhance particle concentration in Ultra fine region with peak lying at 9.3 nm (particle size <50nm). The particle size distribution for rest of the events have mode in fine particle region (PM_{2.5}).

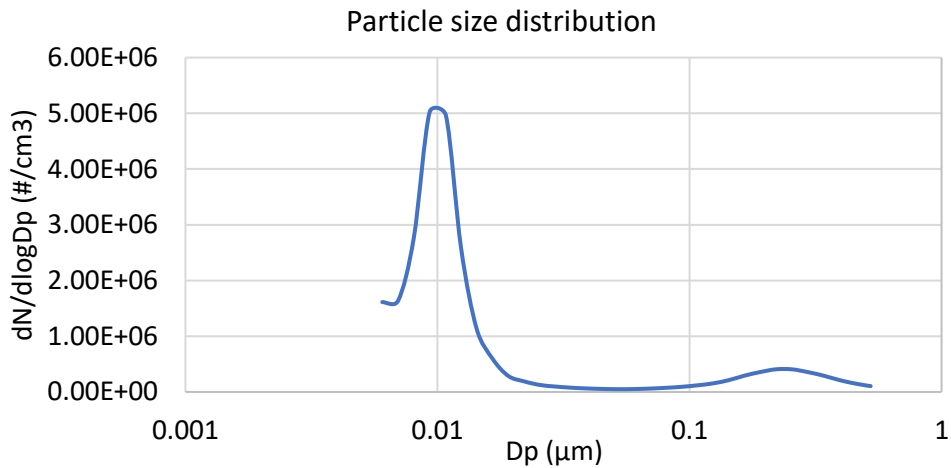


Figure 6.35 Particle size distribution in highest energy dissipation brake event of WLTC

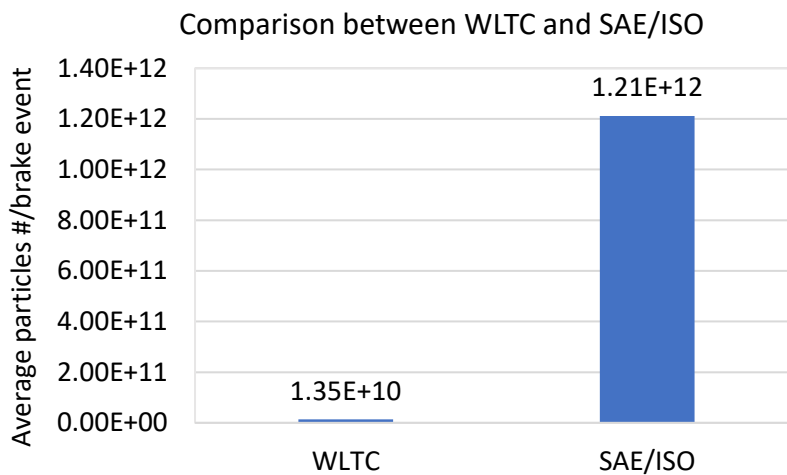


Figure 6.36 Comparison of average particle emissions on WLTC and SAE/ISO of Zimmerman V pad

Figure 6.36 shows the average particle emissions from Zimmerman V brake pad evaluated on WLTC and SAE/ISO test procedures. Since the test procedure SAE/ISO were harsher and more extreme, the particles emitted from each braking event were greater in number and hence the average particles emitted were two orders more than average emissions from WLTC cycle. Figure 6.37 shows the particles emitted per kJ of energy dissipation. The particles/kJ are higher with SAE/ISO procedures as expected.

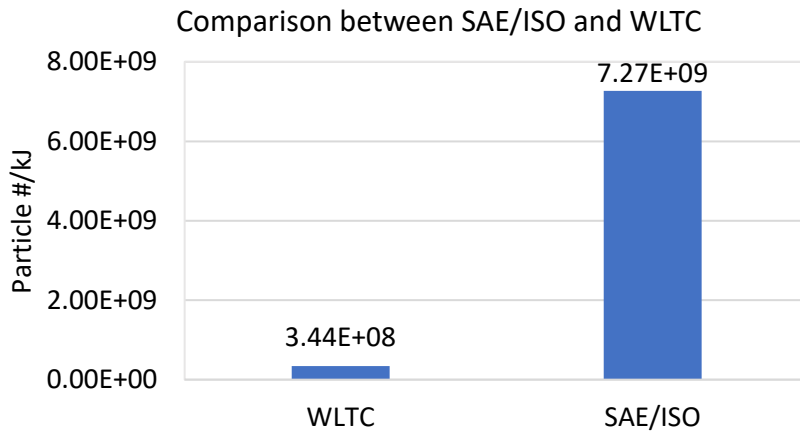


Figure 6.37 Comparison of particle emissions/kJ on WLTC and SAE/ISO of Zimmerman V pad

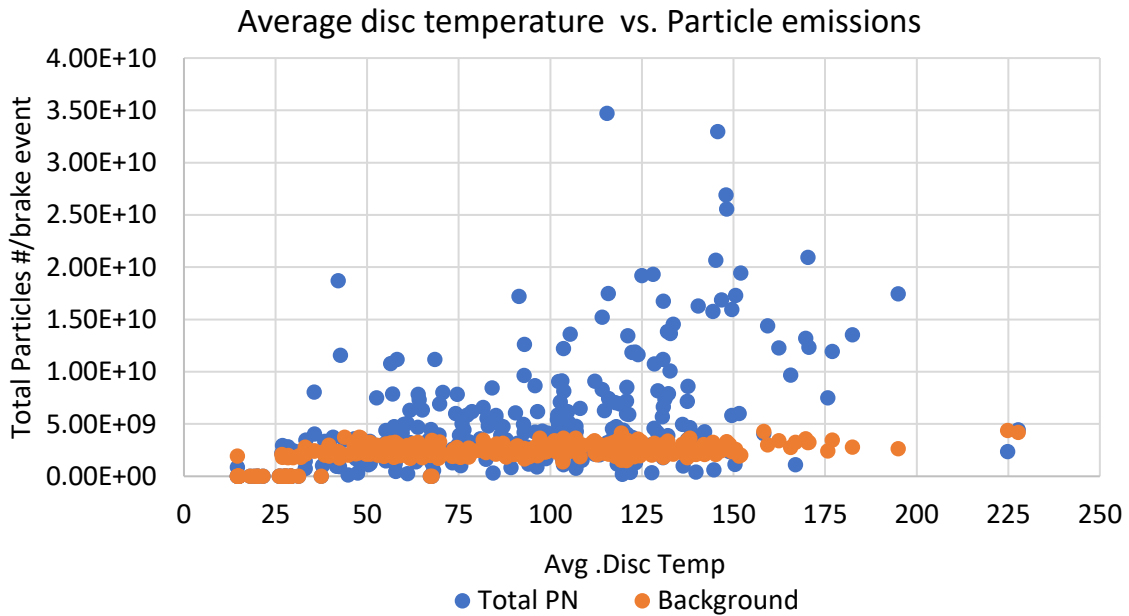


Figure 6.38 Particle number emissions with regards to average disc temperature (EEPS)

Figure 6.38 shows the particle number emissions from the WLTC cycle with respect to average disc temperature on Zimmerman V pad. The particle emissions from majority of the braking events were at the background level of around $\sim 5 \times 10^9$ and there was a moderate rise in emissions with increase in average temperature. Figure 6.39 shows particles produced per kJ of energy dissipated with regards to average disc temperature.

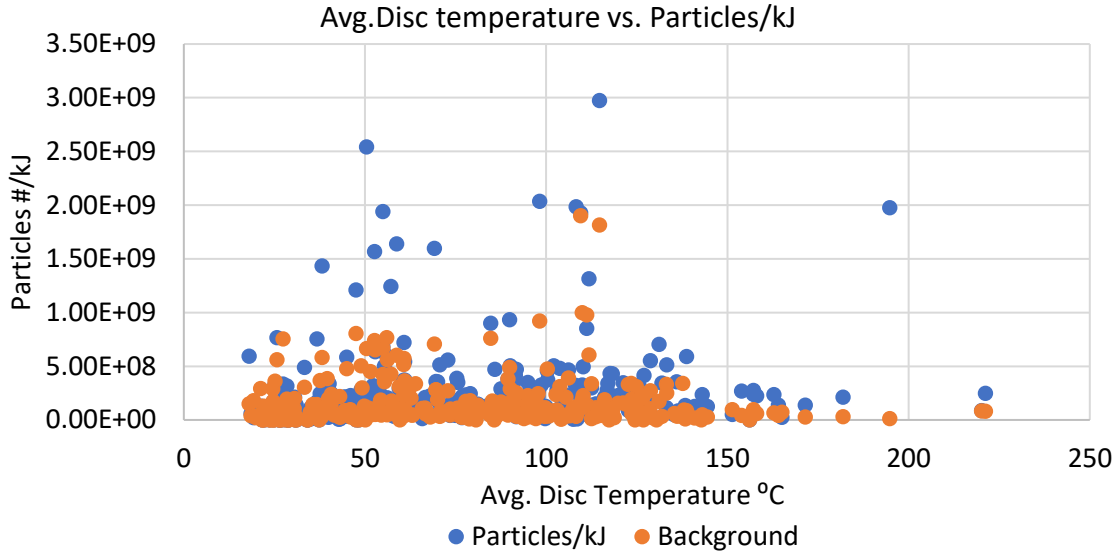


Figure 6.39 Particle emissions/kJ with regards to average disc temperature (Zimmerman V)

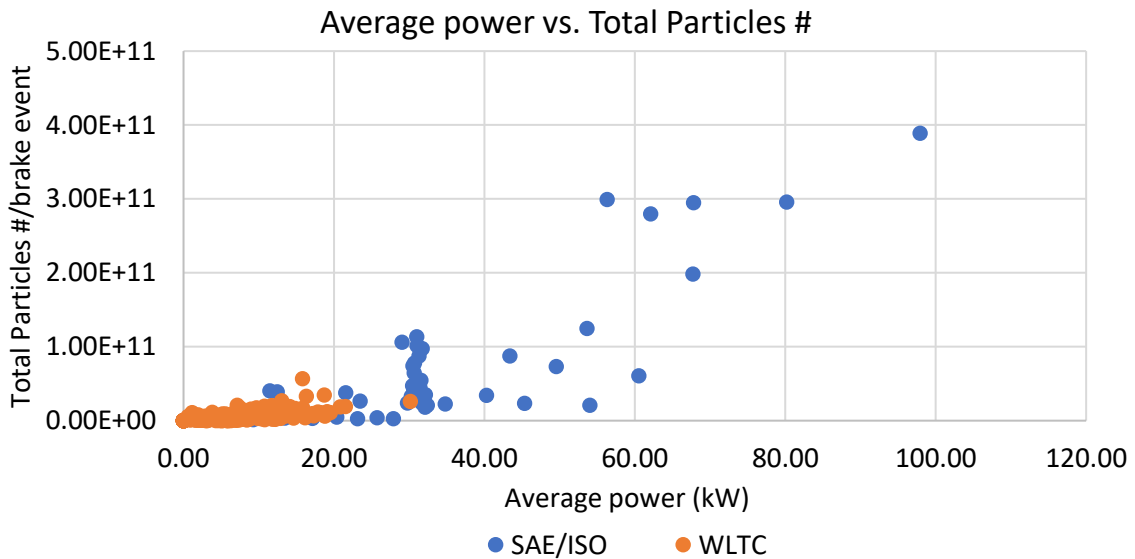


Figure 6.40 Comparison of particle emissions with regards to average power (Zimmerman V)

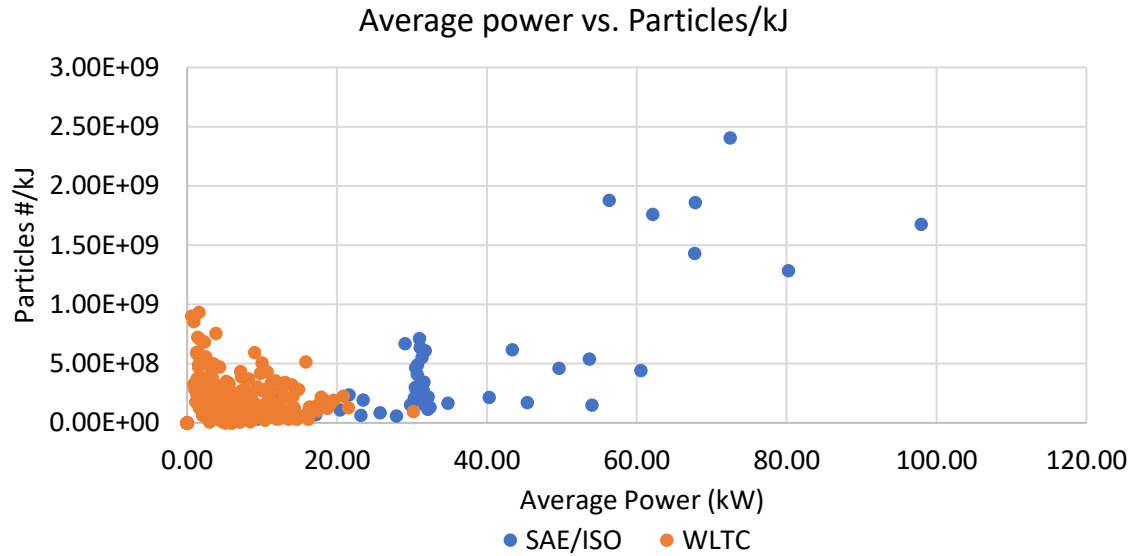


Figure 6.41 Comparison of particle emissions/kJ with regards to average power (Zimmerman V)

Figure 6.40 and figure 6.41 shows the particle emission in terms of total particles emitted and particles per kJ of energy dissipated from the test procedures SAE/ISO and WLTC cycle with regards to average power dissipation. Zimmerman V was used in both the test procedures and WLTC cycle for better comparison. Particle emissions in the orders of 10^{12} and above of SAE/ISO were not shown here for better graphical representation. As the test procedures ISO 26867 and SAE J2522 were more intense compared to WLTC and this was derived from normal road driving data, the particle emissions over WLTC were at the orders of 10^{10} and below with almost negligible particles in Ultra fine region (except for one braking event described above). From the above 2 figures it is clear that average power dissipated in WLTC is less than 20 kW and therefore the particle emissions were lower when compared to SAE/ISO test procedures which operate brake pads under rigorous conditions.

7 Conclusion

The main target of the thesis was to analyze the data from the brake wear particle measurement campaign comprising of four different brake pads chosen as the most popular commercially available pads for a typical midsize passenger automobile. The testing was done on a full scale Inertia brake dynamometer at Technical University of Ostrava. The test sequence consisted of portions of standardized tests, selected as reasonable for real operation of vehicle. On one set of pads, the WLTC brake cycle, a newly developed cycle for brake wear particle measurements was replicated. Particle concentrations in the outlet tunnel of the brake enclosure were measured online at 1 Hz resolution by two particle classifiers, EEPS and ELPI.

Firstly, the data obtained from the instruments were processed by differentiating useful signal from the background noise which consists of instrument noise and particles in the cooling air. The particle emissions were calculated by peak area approach (numerical integration of concentrations multiplied by the total flow in the duct) for all the braking events of the four brake pads, the dependence of particle concentrations on key braking parameters - average brake line pressure, initial and final disc temperatures, average dissipated power and total energy dissipated were investigated. It was found that particles emitted from the brake pad depends on the pad material composition and the operating conditions of the brake.

It is observed that particle emissions rise with an increase in disc temperature. This increase in particle number was significant in the fine particulate region ($PM_{2.5}$) as shown in *figure 6.22* for Original, *figure 6.26* for ABE and *figure 6.30* for Zimmerman pad. A rise in particle emission was also associated with an increase in dissipated power and work, primarily in the ultra fine particulate matter ($PM_{0.1}$). Ferodo, ABE and Original, but not Zimmerman, - brake pads had shown strong correlation of particle emission rise with increase in average power and energy dissipation as shown in *figure 6.10*, *figure 6.11*, *figure 6.12* and *figure 6.13*. Another set of Zimmerman pad labelled as 'Zimmerman V' was used on a novel brake cycle called as brake WLTC to measure and quantify brake wear particle

emissions in real world braking conditions. The particle production over sections of the WLTC cycle was mostly on the order of 10^{10} particles per km, with a value of 1.65×10^{10} particles per km averaged for 3 WLTC tests as shown in *figure 6.33*, which is far lower than the particles produced on standardized cycles. The data from ELPI of WLTC could not be presented here as particle production was low for less intense braking events and hence could not be differentiated from noise of the instrument.

Discussion and Suggestion

The data collected at the brake wear measurement campaign from ELPI and EEPS was analyzed using peak area approach after differentiating useful signal and unwanted noise by creating detection limit and eliminating background noise. It was clearly evident that particle emissions from brake pad depends upon its manufacturer's pad composition and braking conditions. Zimmerman brake pad had highest average particle emissions per brake event and highest particles per kJ of energy dissipated. On the other hand, Original brake pad had the lowest particle emissions in terms of average particles per brake event and per kJ of energy dissipated.

Non-exhaust emissions are gaining importance as the relative contribution of exhaust emissions to total Particulate matter emission is decreasing because of strict legislation on particles emitted from tail pipe which has limit of 6×10^{11} #/km on WLTC. The particles produced on newly developed brake cycle (brake WLTC) with 'Zimmerman V' brake pad produced around $\sim 1-2 \times 10^{10}$ #/km which is lesser compared to tail pipe emissions. Extreme braking events produced particles in the orders of $\# 10^{11}$ which was shown in *figure 6.35*. So, people driving a passenger car, or any sort of vehicle should be aware that intense and harsh braking of the vehicle creates ultra fine particulate matter which effects human health and environment. Being conscious while braking and minimizing rigorous braking events by using engine braking wherever possible can help up to certain level. Brake pad manufacturers should also look for pad formulations and materials to minimize the effects on air quality.

The pads Original, ABE and Ferodo can also be tested on this novel test cycle to see if the emission rate per km is same as Zimmerman V. As Original pad has lowest particle emissions per brake event on SAE/ISO test procedures, this pad can be tested on the brake WLTC to see if it produces any lower particles emissions per km.

Bibliography

- [1] F. Amato, "Urban air quality: the challenge of traffic non-exhaust emissions," *Journal of hazardous materials*, vol. 275, p. 31-36, 2014.
- [2] World Health Organization, "WHO Air quality guidelines for particulate matter, ozone, sulphur dioxide, nitrogen dioxide," WHO, Geneva, 2006.
- [3] H. Hagino, "Laboratory testing of airborne brake wear particle emissions using a dynamometer system under urban city driving cycles," *Atmospheric Environment*, pp. 269-278, 2016.
- [4] European Commission, "European Commission," [Online]. Available: https://ec.europa.eu/growth/sectors/automotive/environment-protection/emissions_en. [Accessed 10 6 2020].
- [5] T. Martini and G. Giorgio, "Brake wear particle emissions: a review," *Environmental Science and Pollution Research*, p. 2491–2504, 2014.
- [6] United States Environmental Protection Agency, "United States Environmental Protection Agency," [Online]. Available: <https://www.epa.gov/report-environment>. [Accessed 10 6 2020].
- [7] United States Environmental Protection Agency, "United States Environmental Protection Agency," [Online]. Available: <https://cfpub.epa.gov/roe/indicator.cfm?i=9>. [Accessed 10 6 2020].
- [8] European Environmental Agency, "Air Quality in Europe," Copenhagen, 2013.
- [9] World Health Organization, "Health Aspects of Air Pollution with Particulate Matter, Ozone and Nitrogen Dioxide," Bonn, 2003.
- [10] F. J. Kelly and J. C. Fussell, "Size, source and chemical composition as determinants of toxicity attributable," *Atmospheric Environment*, vol. 60, pp. 504-526, 2012.
- [11] X. G. Chang Ping, "A review of the health effects and exposure-responsible relationship of diesel particulate matter for underground mines," *International Journal of Mining Science and Technology*, 2017.
- [12] J. C. Abhishek Tiwary, *Air pollution measurement, modelling and mitigation*, Oxon: Routledge, 2010.
- [13] World Health Organization, "World Health Organization," 2018. [Online]. Available: <https://www.who.int/airpollution/data/en/>. [Accessed 11 08 2020].
- [14] M. Loxham, Nieuwenhuijsen and M.J., "Health effects of particulate matter air pollution in underground railway systems – a critical review of the evidence," *Part Fibre Toxicol*, vol. 16, no. 12, 2019.

- [15] "Information about nanomaterials and their safety assessment," Federal Ministry of Education and Research, [Online]. Available: <https://www.nanopartikel.info/en/nanoinfo/body-barriers/2388-nanoparticles-and-the-lung#literatur>. [Accessed 18 6 2020].
- [16] UNECE, "Sustainable development goals," [Online]. Available: <http://www.unece.org/environmental-policy/conventions/envlrapwelcome/cross-sectoral-linkages/air-pollution-ecosystems-and-biodiversity.html>. [Accessed 18 6 2020].
- [17] D. T. Bralower and D. D. Bice, "Earth in the future," College of Earth and Mineral Science, The Pennsylvania State University, [Online]. Available: <https://www.e-education.psu.edu/earth103/node/717>. [Accessed 18 6 2020].
- [18] European Environment Agency, "Sector share for emissions of primary PM2.5 and PM10 particulate matter," 06 05 2015. [Online]. Available: https://www.eea.europa.eu/data-and-maps/daviz/sector-split-of-emissions-of-4#tab-chart_1. [Accessed 5 06 2020].
- [19] European Environmental Agency, "Air Quality in Europe," Denmark, 2019.
- [20] T. Grigoratos and G. Martini, "Non-exhaust traffic related emissions. Brake and tyre wear PM," European Commission, Luxembourg, 2014.
- [21] F. Puhn, Brake Handbook, U.S.A: HP Books.
- [22] Akebono brake industry, "Akebono," [Online]. Available: https://www.akebono-brake.com/english/product_technology/product/automotive/disc/. [Accessed 12 7 2020].
- [23] A. Thorpe and R. M. Harrison, "Sources and properties of non-exhaust particulate matter from road traffic: a review," *SCIENCE OF THE TOTAL ENVIRONMENT*, vol. 400, pp. 270-282, 2008.
- [24] N. Bukowiecki and R. Gehrig, "PM10 emission factors of abrasion particles from road traffic (APART)," in *Swiss Association of Road and Transportation Experts (VSS)*, 2009.
- [25] B. D. Garg, S. H. Cadle and P. A. Mulawa, "Brake Wear Particulate Matter Emissions," *Environmental Science & Technology*, vol. 34, pp. 4463-4469, 2000.
- [26] D. Chan and G. W. Stachowiak, "Review of automotive brake friction materials," *Journal of Automobile Engineering*, vol. 218, pp. 953-966, 2004.
- [27] ITT Motion Technologies, "Wear & Particle emissions control in brake pads".
- [28] Dekati, "products," [Online]. Available: <https://www.dekati.com/products/elpi/>. [Accessed 26 6 2020].
- [29] TSI, "Products," [Online]. Available: https://tsi.com/getmedia/a01ec52e-f39f-4312-8f9a-fded71631a69/3090_Engine_Exhaust_Particle_Sizer_A4_2980351_WEB?ext=.pdf. [Accessed 26 6 2020].

- [30] International Organization for Standardization, "ISO 26867:2009," [Online]. Available: <https://www.iso.org/standard/43848.html>. [Accessed 20 7 2020].
- [31] SAE Mobilus, "Dynamometer Global Brake Effectiveness," [Online]. Available: https://saemobilus.sae.org/content/j2522_201409. [Accessed 20 7 2020].
- [32] Stop Tech, "Pad and Rotor Bed-In Theory, Definitions and Procedures," Centric Parts, Carson.
- [33] M. Marcel and J. Grochowicz, "A novel real-world braking cycle for studying brake wear particle emissions," *Wear*, Vols. 414-415, pp. 219-226, 2018.
- [34] Black hills state university, [Online]. Available: <https://www.bhsu.edu/Portals/91/InstrumentalAnalysis/StudyHelp/LectureNotes/Chapter5.pdf>. [Accessed 15 7 2020].
- [35] E. Theodorsson, "Limit of detection, limit of quantification and limit of blank," EFLM.
- [36] ConsultGLP, "Limit of Detection; Type I (False Positive) and Type II (False negative) errors," GLP Consulting Singapore and Malaysia, Singapore.
- [37] Air Quality Expert Group to the Department for Environment, "Non-Exhaust Emissions from Road Traffic," United Kingdom, 2019.
- [38] W. C. Hinds, *Aerosol Technology: Properties, Behavior, and Measurement of Airborne Particles*, 2nd Edition, Massachusetts: John Wiley and Sons, 1999.
- [39] J. R. Dunshee, "Evaluation Of The Engine Exhaust Particle Sizer for Real Time measurements of Diesel and Biodiesel Exhaust Particulate Matter," University of Vermont, Vermont, 2016.
- [40] J. S. Zhun Liu, "Comparison of Methods for Online Measurement of Diesel Particulate Matter," *Environmental Science and Technology*, vol. 46, pp. 6127-6133, 2012.
- [41] J. O. Anderson, J. G. Thundiyil and A. Stolbach, "Clearing the Air: A Review of the Effects of Particulate Matter Air Pollution on Human Health," *Journal of medical Toxicology*, vol. 8, no. 2, pp. 166-175, 2012.

List of Tables

Table 1.1 Air quality standards for protecting human health for PM10 and PM2.5 [19]	7
Table 4.1 Sections of ISO 26867 testing procedure used in the test.....	17
Table 4.2 Sections of SAE J2522 testing procedure used in the test.....	18

List of Figures

Figure 1.1 Illustration of PM _{2.5} and PM ₁₀ [8].....	2
Figure 1.2 Size distribution of Particles [11]	3
Figure 1.3 Formation of Particulate matter in atmosphere [12].....	4
Figure 1.4 Possible Pathway of PM transport in human lungs [15]	5
Figure 1.5 Sector share of PM _{2.5} and PM ₁₀ emissions [18]	6
Figure 1.6 Observed daily mean concentration of PM ₁₀ [19]	7
Figure 1.7 Disc brake working mechanism [22].....	9
Figure 1.8 Typical Composition of brake pad [26]	10
Figure 3.1 Brake Dynamometer used for the experiment [27]	13
Figure 3.2 Schematic representation of ELPI [28]	14
Figure 3.3 Schematic diagram of EEPS [29]	15
Figure 4.1 Velocity-time schedule of WLTC Brake cycle [33]	20
Figure 4.2 Cumulative frequency distribution of selected sections of ISO and SAE with regards to deceleration	21
Figure 4.3 Cumulative frequency distribution of selected sections of ISO and SAE with regards to initial velocity	21
Figure 5.1 Showing response of EEPS for series of brake events.....	23
Figure 5.2 Enlarged view of a brake event showing Signal and Noise	23
Figure 5.3 Peak areas above detection limit considered for analysis	24
Figure 5.4 Baseline for the Instrument response	25
Figure 5.5 Signal after baseline correction	26
Figure 5.6 Time Synchronizing between ELPI and EEPS	27
Figure 5.7 Particle size distribution (EEPS)	29
Figure 5.8 Lognormal particle size distribution (EEPS)	29
Figure 5.9 Particle size distribution in ELPI.....	30
Figure 5.10 Particle size distribution in EEPS.....	31
Figure 5.11 Comparison of Normalized particle size distribution in EEPS and ELPI.....	31

Figure 5.12 Comparison of Mass distribution in EEPS and ELPI	33
Figure 6.1 Average particles emitted from brake pads	34
Figure 6.2 Particle emissions on test section F	35
Figure 6.3 Average Particle Size Distribution - Section F	36
Figure 6.4 Particle emissions on test section G	37
Figure 6.5 Average Particle Size Distribution - Section G	38
Figure 6.6 Particle emissions on test section H	38
Figure 6.7 Average Particle Size Distribution - Section H	39
Figure 6.8 Particle emissions on test section K.....	40
Figure 6.9 Average Particle Size Distribution - Section K.....	41
Figure 6.10 Dependence of total particles emitted on average power (Original)	42
Figure 6.11 Dependence of total particles emitted on average power (ABE).....	42
Figure 6.12 Dependence of total particles emitted on average power (Zimmerman V)	43
Figure 6.13 Dependence of total particles emitted on average power (Ferodo).....	44
Figure 6.14 Particles emissions at highest average power dissipation	44
Figure 6.15 Comparison of particle emissions with respect to unit energy dissipation	45
Figure 6.16 Particles/kJ emitted with respect to average power dissipation (Original)	46
Figure 6.17 Particles/kJ emitted with respect to average power dissipation (ABE)	46
Figure 6.18 Particles/kJ emitted with respect to average power dissipation (Zimmerman V)	47
Figure 6.19 Particles/kJ emitted with respect to average power dissipation (Ferodo)	47
Figure 6.20 Particle emissions with regards to temperature of disc (Original).....	48
Figure 6.21 Particle emissions per kJ of energy dissipated (Original)	48
Figure 6.22 Variation of particle size distribution with respect to temperature (Original)	49
Figure 6.23 Variation of Mass distribution with respect to temperature (Original)	50
Figure 6.24 Particle emissions with regards to temperature of disc (ABE)	50
Figure 6.25 Particle emissions per kJ of energy dissipated (ABE).....	51
Figure 6.26 Variation of particle size distribution with respect to temperature (ABE).....	51
Figure 6.27 Variation of Mass distribution with respect to temperature (ABE)	51
Figure 6.28 Particle emissions with regards to temperature of disc (Zimmerman).....	52

Figure 6.29 Particle emissions per kJ of energy dissipated (Zimmerman) 52

Figure 6.30 Variation of particle size distribution with respect to temperature (Zimmerman) .. 53

Figure 6.31 Variation of Mass distribution with respect to temperature (Zimmerman) 53

Figure 6.32 Particle emissions in each segment of WLTC 54

Figure 6.33 Particle emissions over 3 repeated WLTC cycles (EEPS)..... 55

Figure 6.34 Particulate mass over the WLTC cycle calculated from EEPS 55

Figure 6.35 Particle size distribution in highest energy dissipation brake event of WLTC..... 56

Figure 6.36 Comparison of average particle emissions on WLTC and SAE/ISO of Zimmerman V pad 56

Figure 6.37 Comparison of particle emissions/kJ on WLTC and SAE/ISO of Zimmerman V pad. 57

Figure 6.38 Particle number emissions with regards to average disc temperature (EEPS) 57

Figure 6.39 Particle emissions/kJ with regards to average disc temperature (Zimmerman V) ... 58

Figure 6.40 Comparison of particle emissions with regards to average power (Zimmerman V). 58

Figure 6.41 Comparison of particle emissions/kJ with regards to average power (Zimmerman V) 59

Appendix

EEPS Bin Designations

Bin number	Bin Min D_p(nm)	Bin Midpoint D_p(nm)	Bin Max D_p(nm)	dlogD_p
B1	5.61	6.04	6.48	0.06
B2	6.48	6.98	7.48	0.06
B3	7.48	8.06	8.64	0.06
B4	8.64	9.31	9.98	0.06
B5	9.98	10.75	11.52	0.06
B6	11.52	12.41	13.3	0.06
B7	13.3	14.33	15.36	0.06
B8	15.36	16.55	17.74	0.06
B9	17.74	19.11	20.48	0.06
B10	20.48	22.065	23.65	0.06
B11	23.65	25.48	27.31	0.06
B12	27.31	29.42	31.54	0.06
B13	31.54	33.98	36.42	0.06
B14	36.42	39.24	42.06	0.06
B15	42.06	45.31	48.57	0.06
B16	48.57	52.33	56.09	0.06
B17	56.09	60.43	64.77	0.06
B18	64.77	69.78	74.79	0.06
B19	74.79	80.58	86.37	0.06
B20	86.37	93.05	99.74	0.06
B21	99.74	107.46	115.18	0.06
B22	115.18	124.09	133	0.06
B23	133	143.29	153.59	0.06
B24	153.59	165.48	177.37	0.06
B25	177.37	191.09	204.82	0.06
B26	204.82	220.67	236.52	0.06
B27	236.52	254.82	273.13	0.06
B28	273.13	294.27	315.41	0.06
B29	315.41	339.82	364.23	0.06
B30	364.23	392.42	420.61	0.06
B31	420.61	453.16	485.71	0.06
B32	485.71	523.3	560.89	0.06

ELPI Bin Designations

Bin Number	D50% Lower cut off (μm)	D50% Upper cut off (μm)	dlogDp
B14	5.3	10	0.28
B13	3.6	5.3	0.17
B12	2.5	3.6	0.16
B11	1.6	2.5	0.19
B10	0.94	1.6	0.23
B9	0.60	0.94	0.19
B8	0.38	0.60	0.20
B7	0.25	0.38	0.18
B6	0.15	0.25	0.22
B5	0.094	0.15	0.20
B4	0.054	0.094	0.24
B3	0.030	0.054	0.26
B2	0.016	0.030	0.27
B1	0.006	0.016	0.43

ELPI Instrument Specifications

Particle size range	0.006 - 10 μm
Number of channels	14 electrically detected + preseparator stage
Sampling rate	10 Hz
Nominal air flow	10 l/min
Ambient temperature	10-35 $^{\circ}\text{C}$
Sample conditions gas temperature	< 60 $^{\circ}\text{C}$
Electric power	100-250 V, 50-60 Hz, 200 W
Charger voltage	3.5 kV +/- 0.5 kV
Charger current	1 μA
Pump requirements	Minimum 16 m ³ /h @ 40 mbar
Computer requirements	MS-Windows 7, MS-Windows 8, MS-Windows 10
Connection to PC	RS-232 or Ethernet
3 analogue inputs	0-10 V
6 analogue outputs	0-10 V

EEPS Instrument Specifications

Particle Size Range	5.6 to 560 nm
Particle Size Resolution	16 channels per decade (32 total)
Electrometer Channels	22
Charger Mode of Operation	Unipolar diffusion charger
Inlet Cyclone 50% Cut point	1 μm
Time Resolution	10 size distributions/sec
Sample Flow	10 L/min
Sheath Air	40 L/min
Inlet Sample Temperature	10 to 52 $^{\circ}\text{C}$
Operating Temperature	0 to 40 $^{\circ}\text{C}$
Storage Temperature	-20 to 50 $^{\circ}\text{C}$
Atmospheric Pressure Correction Range	70 to 103 kPa (700 to 1034 mbar)
Humidity	0 to 90% RH (noncondensing)
Computer Requirements	Pentium 4 processor, 2 GHz speed or better, at least 512 MB RAM
Power Requirements	100 to 240 VAC, 50/60 Hz, 250W